JOURNAL OF SOLID STATE CHEMISTRY 88, 115–139 (1990)

Crystal Chemistry and Superconductivity of the Copper Oxides

J. B. GOODENOUGH AND A. MANTHIRAM

Center for Materials Science and Engineering, ETC 5.160, The University of Texas at Austin, Austin, Texas 78712

Received April 16, 1990

DEDICATED TO J. M. HONIG ON THE OCCASION OF HIS 65TH BIRTHDAY

This paper highlights the important roles played by crystal chemistry in controlling the superconductive properties of the intergrowth structures of the copper oxides. Bond-length matching across the intergrowth interface stabilizes at least four different structures—T/O, T′, T*, and T″—in the simplest system $La_{2-y}Ln_yCuO_4$ (*Ln* = lanthanide) depending upon the size of *Ln* and the value of *y*. The internal electric field created by the formal charges in the adjacent layers modulates the distribution of holes between the active and inactive layers and the influence of Pr on superconductivity. The coordination geometry preferred by different oxidation states of Cu appears to control the oxygen ordering and the T_c variation in the $YBa_2Cu_3O_{6+x}$ system. The *c*-axis Cu–O distance modulates the width of the conduction band and the electronic properties. Chemical characterization of the thallium cuprates has demonstrated that the oxidation of the $Tl_{2-y}Ba_2Ca_{n-1}Cu_nO_{2n+4-x}$ system can be due to either solely an overlap of the Tl: 6*s* band with the conduction band or solely Tl vacancies, depending upon the value of *y*; as normally prepared, both effects are operative.

I. Introduction

The known copper-oxide superconductors all have the following features in common (*1*):

(1) Intergrowth structures consisting of superconductively active layers containing CuO_2 sheets with a constant oxygen concentration and inactive layers of variable oxygen concentration.

(2) Superconductor compositions have a mixed valence in the CuO_2 sheets and occur in a narrow compositional range between a small-polaron conductor and a normal-metal conductor.

(3) Superconductor compositions exhibit short-range spin fluctuations in the CuO_2 sheets and occur in a narrow compositional range between an antiferromagnetic semiconductor and a Pauli paramagnetic metal.

(4) The nearly 180° Cu–O–Cu interactions in the CuO_2 sheets give a conduction band of width $W \sim \varepsilon_\sigma(\lambda_\sigma^2 + \lambda_s^2)$, where ε_σ is a one-electron energy and λ_σ, λ_s are covalent-mixing parameters for the Cu–$3d_{x^2-y^2}$ and O–$2p_{\sigma x}$, $2p_{\sigma y}$ or O–2*s* hybridizations, respectively; and the values of λ_σ, λ_s appear to increase dramatically with increasing concentration of mobile holes in the CuO_2 sheets of the *p*-type superconductors because the charge-transfer equilibrium

$$Cu^{3+} + O^{2-} \rightleftarrows Cu^{2+} + O^- \qquad (1)$$

is increasingly biased to the right with increasing hole concentration.

0022-4596/90 $3.00

(5) A strong tetragonal component of the crystalline field at the Cu sites in a CuO_2 sheet removes the orbital degeneracy of the conduction band of Cu–3*d* parentage; it is a nondegenerate $\sigma^*_{x^2-y^2}$ band that is half-filled for a formal valence Cu^{2+} on the copper atoms.

We believe that any model of the electron pairing in the superconductive state must take into account the confluence of all these factors, and a "correlation-bag" model that does so has been suggested (*2*). This model introduces charge fluctuations as an expression of electronic instabilities where the on-site correlation energy U is too large for stabilization of a "negative U" charge-density wave, and it utilizes the sensitivity of the bandwidth and correlation energies to the mobile-charge concentration to obtain a binding energy for the Cooper pairs that supplements the electron–phonon interactions responsible for the charge fluctuations.

In this paper we highlight a few aspects of the crystal chemistry of these systems; the chemistry—including the synthesis, characterization, and structure–property relationships—of this class of materials has been presented in an earlier review (*3*). In Section II, we point out the role of bond-length mismatch at the interlayer interfaces in determining the phase relationships in systems with Ln_2CuO_4 end members; in Section III the influence of the mobile oxygen in the inactive layers on the distribution of holes between active and inactive layers is described; in Section IV the influence of Pr on the superconductivity is presented as an illustration of the significance of the positioning of a $4f^n$ configuration relative to the Fermi energy; and in Section V a wet-chemical procedure for determining both the Tl and oxygen contents of the thallium cuprates is outlined and utilized to contrast the properties of the thallium and bismuth cuprates.

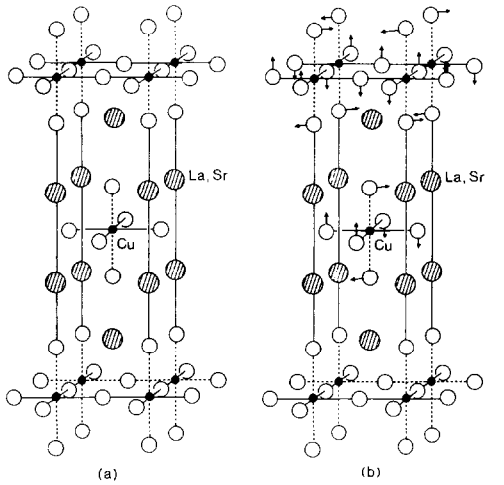

FIG. 1. Structures of (a) tetragonal (T) and (b) orthorhombic (O) La_2CuO_4. The arrows indicate the direction of the tilting of the CuO_6 octahedra.

II. Phase Relationships in Systems with Ln_2CuO_4 End Members

A. End-Member Phases Ln_2CuO_4

The prototype *p*-type and *n*-type copper oxide superconductors have the simplest intergrowth structures with an ideal chemical formula Ln_2CuO_4 for a system end member.

1. La_2CuO_4. The compound La_2CuO_4 crystallizes in the tetragonal structure of Fig. 1a at high temperatures; it undergoes a displacive transition to orthorhombic symmetry below a transition temperature T_t in which the CuO_6 octahedra are rotated cooperatively about a [110] axis as indicated by the arrows in Fig. 1b (*4*). In this structure, the layer that becomes superconductively active with *p*-type doping consists of a single CuO_2 sheet; the inactive layers of variable oxygen content consist of the two (001) rocksalt planes of the $(LaO)_2$ layers. We denote the layer sequence along the *c*-axis as

$$|CuO_2|LaO–LaO|CuO_2| \qquad (2)$$

where the vertical lines mark the interlayer interfaces.

Such an intergrowth imparts three important properties to the compound:

—Its physical properties are strongly anisotropic.

—Where the layers are alternately charged positively and negatively—in La_2CuO_4 the CuO_2 sheets carry a formal charge 2− and the $(LaO)_2$ layers a charge 2+ per formula unit—an internal electric field exists that lowers the electronic energy levels in the positively charged layers and raises them in the negatively charged layers.

—Bond-length mismatch across the interface creates a tensile stress within one layer and a compressive stress in the other. A measure of the bond-length matching is the Goldsmidt tolerance factor

$$t = (\text{La–O})/\sqrt{2}(\text{Cu–O}), \qquad (3)$$

where the La–O and Cu–O bond lengths are commonly taken as the sums of the empirically determined room-temperature ionic radii. Ideal matching occurs for $t = 1$. However, a larger thermal expansion for the La–O versus the Cu–O bond means that t decreases with decreasing temperature. Therefore, although a $t \approx 1$ may be approached at the temperature of phase formation, a $t < 1$ at lower temperatures places the $(LaO)_2$ layers under tension and the CuO_2 sheets under compression. Nature adjusts to this bond-length mismatch in three successive steps in La_2CuO_4: First, it orders the single Cu–3d hole at a Cu^{2+} ion into the $3d_{x^2-y^2}$ orbital (z-axis taken parallel to c-axis), which results in a large tetragonal ($c/a > 1$) distortion of the CuO_6 octahedra. Second, interstitial oxygen atoms tend to be introduced between the LaO planes of an $(LaO)_2$ layer (*5–9*); they occupy sites coordinated by four La and four c-axis O (*8, 9*). Third, a cooperative tilting of the CuO_6 octahedra below T_t buckles the CuO_2 sheets in the orthorhombic structure; bending of the Cu–O–Cu bond from 180° relieves the compressive stress on the CuO_2 sheets.

2. Ln_2CuO_4, Ln = Pr, . . . Gd. Replacement of the larger La^{3+} ion by a smaller lanthanide ion *Ln* = Pr, . . . Gd increases the bond-length mismatch for the La_2CuO_4 structure, which we designate the T/O structure, by reducing t; in this case, nature responds by a displacement of the c-axis oxygen of Fig. 1a to the plane of tetrahedral sites in the $(LnO)_2$ layer to give a fluorite layer in place of the rocksalt layer (*10*) (Fig. 2a):

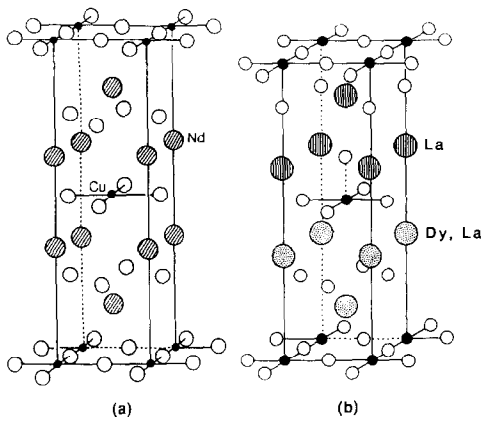

FIG. 2. Structures of (a) T′ − Nd_2CuO_4 and (b) T*-$La_{2-y}Dy_yCuO_4$.

$$|CuO_2|Ln\text{–}O_2\text{–}Ln|CuO_2|. \qquad (4)$$

The electrostatic repulsions between the coplanar oxygen in the fluorite layer expand the a-axis sufficiently to place the CuO_2 sheets under tension, and 180° Cu–O–Cu bonds are retained to the lowest temperatures (*11*). The tetragonal structure of Fig. 2a is designated the T′ structure to distinguish it from the T/O structure of Fig. 1.

The T′ structure does not support a buckling of the CuO_2 planes to bend the 180° Cu–O–Cu bond angle; therefore, the range of Ln^{3+} ionic radii that the phase can tolerate is Pr^{3+} . . . Gd^{3+}, and in Gd_2CuO_4 we may anticipate that the CuO_2 sheets experience little tension at lower temperatures. CuO_2 sheets under compression in the T/O structure are readily doped p-type, but not

n-type; CuO_2 sheets under tension in the T′ structure are readily doped n-type, but not p-type. In addition, the stability of a higher formal valence on the copper increases with its anion coordination, and the Cu in the p-type T structure are sixfold-coordinated whereas those in the n-type T′ structure are only fourfold-coordinated.

B. Mixed Rare Earth Systems $La_{2-y}Ln_yCuO_4$

If a larger La^{3+} ion is partially replaced by a significantly smaller rare earth ion Ln^{3+} (Ln = Sm, . . . Dy), bond-length mismatch makes difficult stabilization of either a pure T or T′ structure; instead a new hybrid structure, designated T*, is stabilized (*12–14*). The T* structure, illustrated in Fig. 2b, contains alternating La-rich rocksalt layers and Ln-rich fluorite layers:

$$|CuO_2|LaO\text{–}LaO|CuO_2|La,Ln\text{–}O_2\text{–}$$
$$La,Ln|CuO_2|. \quad (5)$$

A nearly perfect interlayer ordering of La^{3+} and Ln^{3+} ions is generally found for $y \approx 1$ in $La_{2-y}Ln_yCuO_4$ with Ln = Tb or Dy. Only the Ln^{3+} ions smaller than Sm^{3+} provide a fluorite layer compatible with a rocksalt $(LaO)_2$ layer. In this structure the copper have fivefold oxygen coordination, and the T* phases can be doped p-type; they also exhibit a bending of the Cu–O–Cu bonds from 180° at low temperatures as a result of different bonding to fluorite versus rocksalt adjacent planes (*12–14*).

On the other hand, if the larger La^{3+} ion is partially replaced by a lanthanide ion of more compatible size (Ln = Pr or Nd), then a disordering of the La^{3+} and Ln^{3+} ions within a rocksalt or a fluorite layer becomes feasible; the T phase tolerates a considerable solid–solution of Pr or Nd in La_2CuO_4 and the T′ phase of La in Pr_2CuO_4 or Nd_2CuO_4, and the interlayer ordering characteristic of the T* phase does not occur. Figure 3 shows the variation of the room temperature lattice parameters versus the composition y—or a calculated tolerance factor t—for the system $La_{2-y}Nd_yCuO_4$ that was obtained by firing the component oxides at 1060°C followed by annealing in 1 atm O_2 (*15*). In the construction of this diagram, the t values were calculated from the room temperature ionic radii with Cu^{2+} in octahedral coordination—a choice of square-coplanar coordination would shift all t values in Fig. 3, but make no other change—and La^{3+}, Ln^{3+} in nine-fold coordination (*16*). The orthorhombic La_2CuO_4 structure is found for $0 \leq y \leq 0.35$ and $t \geq 0.8658$, the T′–Nd_2CuO_4 structure for $1.2 \leq y \leq 2.0$ and $t \leq 0.8585$. The T′ structure has a smaller c-axis and a larger a-axis than the T structure;

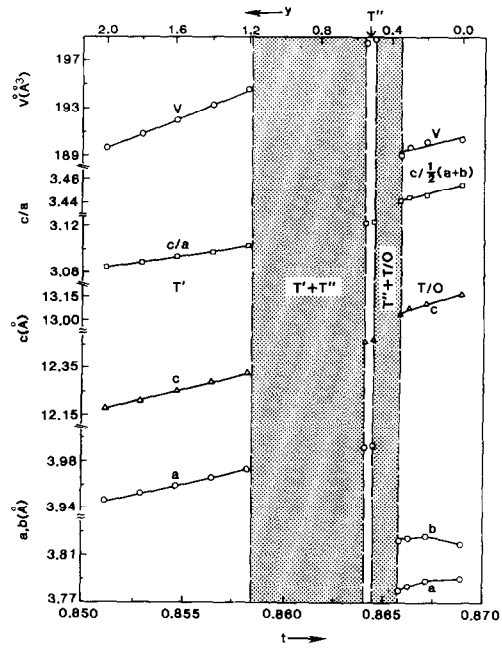

FIG. 3. Variation of room temperature lattice parameters with t or y for the system $La_{2-y}Nd_yCuO_4$; t values were obtained with the nine-coordinated radius for La^{3+} and Nd^{3+} for all values of y. For comparison, the a and b parameters for the T/O phases are plotted by dividing the actual orthorhombic parameter by $\sqrt{2}$.

it also has a larger cell volume. Instead of a T* phase appearing at $y \approx 1$, a new phase, designated T″, appears at $y \approx 0.5$. For the system Ln = Pr, the T″ phase also appears at $y \approx 0.5$, which suggests that the phase is characterized by an intralayer ordering at a La^{3+}/Ln^{3+} ratio 3 : 1 rather than the interlayer ordering of the T* phase at a La^{3+}/Ln^{3+} ratio 1 : 1.

Identification of the T″ phase is a bit subtle as it has a powder X-ray diffraction pattern similar to that of the T′ phase, but with a slightly larger parameter than that obtained by a Végard's law extrapolation of the lattice constants from the T′ solid–solution phase field. Bringley *et al.* (*17*) did not distinguish the T″ phase from the T′ phase in their study of this system and interpreted the two-phase character of the system at $y \approx 1$ as a manifestation of a stabilization of the T* phase within the T′ phase field. In our study, the intermediate compositional range $0.55 < y < 1.2$ consisted of two phases with powder-diffraction patterns similar to T′, but having distinguishable lattice parameters. The narrow region $0.5 \leq y \leq 0.55$ showed only a single phase with the larger lattice parameter. The appearance of a two-phase region in the interval $0.55 < y < 1.2$ indicates that the phase found at $y = 0.5$ is distinguishable from that in the interval $1.2 \leq y \leq 2.0$ even though they give similar diffraction patterns. Therefore we designate this phase as T″. Because it appears with a limited solid solubility range at $y = 0.5$ for both Ln = Pr and Ln = Nd, we assume it is characterized by an intralayer ordering of the La^{3+} and Ln^{3+} ions; the order may allow a cooperative c-axis displacement of the oxygen atoms in the $La_{1.5}Ln_{0.5}$–O_2–$La_{1.5}Ln_{0.5}$ layers. This assumption has yet to be checked experimentally.

Interestingly, pellets of intermediate composition $0.5 < y < 1.2$ in the $La_{2-y}Nd_yCuO_4$ system that had been quenched in air to room temperature from 1060°C exhibited a spontaneous disintegration into a fine powder within a few minutes at room temperature. This observation is consistent with a disordering of the La^{3+} and Nd^{3+} ions within a fluorite layer at the firing temperature and a "spinodal decomposition" into an ordered and a disordered phase at lower temperatures.

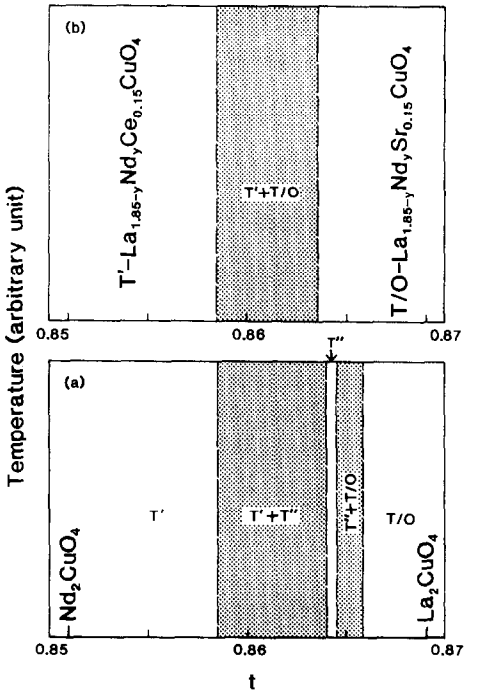

FIG. 4. Phase diagrams for the (a) undoped $La_{2-y}Nd_yCuO_4$ and (b) doped $La_{1.85-y}Nd_ySr_{0.15}CuO_4$ and $La_{1.85-y}Nd_yCe_{0.15}CuO_4$ systems.

The larger a-parameter of the T″ phase suggests that the CuO_2 planes are under tension and might therefore readily be doped n-type, as is the case for the T′ phase. However, doping by the substitution of either La^{3+} or Nd^{3+} by Ce^{4+} or by Sr^{2+} resulted in a disproportionation into an n-type T′ phase and an undoped T phase on the one hand, a p-type T phase and an undoped T′ phase on the other hand. The two situations are illustrated in Fig. 4. This observation is consistent with the postulate of a 3 : 1 cation ordering in the T″ phase; the order is pre-

sumably suppressed by the introduction of a third type of cation.

C. The System $La_{2-y}Sr_yCuO_4$

The end member La_2CuO_4 is an antiferromagnetic semiconductor with a Néel temperature T_N = 326 K that decreases sensitively with the introduction of mobile holes into the CuO_2 sheets (*18*). Substitution of smaller La^{3+} ions by larger Sr^{2+} ions in $La_{2-y}Sr_yCuO_4$ relieves the tensile stress in the (La,Sr)O rocksalt planes, and removal of antibonding electrons from the CuO_2 sheets relieves the compressive stress on the CuO_2 sheets. Also, the Cu are octahedrally coordinated. Consequently *p*-type doping by Sr substitution is readily accomplished (*19, 20*), and the orthorhombic–tetragonal transition temperature T_t decreases with increasing y (*21*). Moreover, the tendency to pick up interstitial oxygen also decreases with increasing y, and annealing in 1 atm O_2 is required to maintain the oxygen stoichiometry as y increases toward y = 0.27 (*22*). At higher values of y, an oxygen partial pressure in excess of 1 atm O_2 is required to maintain the oxygen stoichiometry.

A tentative phase diagram for the system $La_{2-y}Sr_yCuO_4$ is given in Fig. 5. Of particular interest in this system are the following features:

(1) Superconductivity occurs in a narrow, mixed-valent compositional range between an antiferromagnetic semiconductor phase and a normal-metal phase. In the antiferromagnetic semiconductor phase, the width of the $\sigma^*_{x^2-y^2}$ band W is smaller than the intra-atomic correlation energy U for the half-filled band. La_2CuO_4 is therefore characterized by an empty $\sigma^*_{x^2-y^2}$ upper Hubbard band and a filled $\sigma^*_{x^2-y^2}$ lower Hubbard band.

(2) With increasing y, long-range antiferromagnetic order below a Néel temperature T_N disappears for $y \gtrsim 0.03$; a spin-glass state

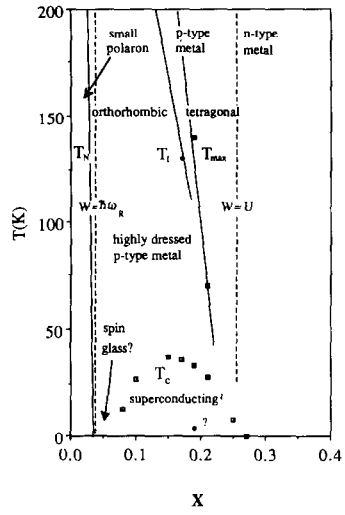

FIG. 5. Phase diagram for the system $La_{2-y}Sr_yCuO_4$.

appears to be stabilized at lowest temperatures in the interval $0.03 < y < 0.06$ where the system undergoes a transition from a small polaron to a metallic conductor (*23*).

(3) From Hall measurements (*24*) the superconductor compositional range, like the small-polaron compositional range, is a *p*-type conductor in the normal state; a change to *n*-type conduction in the normal-metal phase occurring at $y > 0.25$ (*25*) signals a collapse of the correlation splitting into upper and lower $\sigma^*_{x^2-y^2}$ bands (*26*) (see Fig. 6).

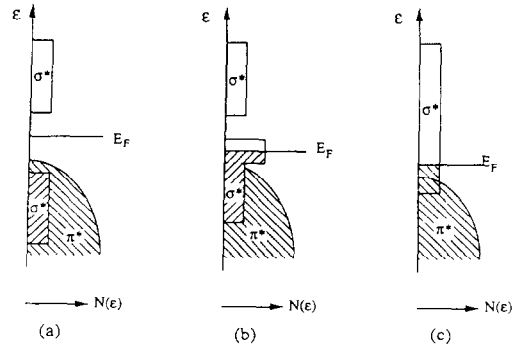

FIG. 6. Idealized energy density of states $N(\varepsilon)$ vs energy ε for (a) La_2CuO_4, (b) $La_{1.85}Sr_{0.15}CuO_4$, and (c) $La_{1.6}Sr_{0.4}CuO_4$.

This deduction is reinforced by the disapperance with increasing y of the maximum in the paramagnetic susceptibility at a temperature T_{max} (*27*), such a susceptibility maximum is characteristic of the onset of short-range spin fluctuations below T_{max} in a two-dimensional spin system, and short-range spin fluctuations have been directly observed by neutron scattering (*28*), muon spin rotation (*29*), nuclear magnetic resource (*30*), and nuclear quadruple resonance (*31*) in the superconductor compositional range.

(4) The change from a $W < U$ to a $W > U$ on varying the mobile-hole concentration p in the CuO_2 sheets over the range $0 < y = p < 0.3$ indicates a remarkable sensitivity of the bandwidth $W \sim \varepsilon_\sigma(\lambda_\sigma^2 + \lambda_s^2)$, and hence of the covalent-mixing parameters λ_σ and λ_s, to the oxidation state of the CuO_2 sheets. This fact and the spectroscopic observation (*32*) of a strong admixture of O-2p character in the conduction band states signals that the equilibrium of Eq. (1) approaches—or may even achieve—crossover with increasing hole concentration $p = y$ in the system $La_{2-y}Sr_yCuO_4$ (*33*).

These data indicate that the superconductor phase occurs in a narrow, mixed-valent compositional range within a nondegenerate band having a width $W \approx U$ and $W \approx 8\hbar\omega_R$, where ω_R^{-1} is the period of the optical-mode lattice vibrations that "dress" a small polaron in a local lattice deformation; moreover W increases remarkably sensitively with hole concentration. This latter sensitivity is made manifest in a room temperature thermoelectric power that decreases exponentially with increasing y (*34–37*).

Finally, there is increasing evidence that the normal state of the superconductor compositions is abnormal below room temperature (*38*) with anomalies in a temperature range near 240 K (*39*) that suggest electron-lattice interactions play an important role. In a mixed-valent system, they can introduce charge fluctuations; these charge fluctuations would represent a dynamic segregation into "bags" of higher hole concentration with $W > U$ within a matrix of lower hole concentration supporting spin fluctuations and a $W < U$. This possibility provides the basis of a recently proposed "correlation-bag" model of superconductivity (*2*).

D. Anion Insertion: La_2CuO_{4+x}

Oxidation of the CuO_2 sheets can also be accomplished by the insertion of interstitial oxygen in the rocksalt layers of La_2CuO_4:

$$|CuO_2|LaO\text{–}O_x\text{–}LaO|CuO_2. \qquad (6)$$

The observation of filamentary superconductivity in La_2CuO_{4+x} compositions was noted early (*40*). Subsequent neutron diffraction studies (*8, 9*) on samples prepared at high oxygen pressures (*6*) have established the existence of two oxygen-rich phases: one corresponds to an $x < 0.02$ and the other to an $x > 0.05$. It remains to be established whether the interstitial oxygen is neutral in the $x < 0.02$ phase, forming one short O–O bond as in a peroxide ion $(O_2)^{2-}$; but it clearly oxidizes the CuO_2 sheets in the $x > 0.05$ phase, which is a p-type superconductor (*6, 41*). In the superconductor phase, the interstitial oxygen is probably an oxide ion O^{2-} with four equivalent O–O bonds as in La_2NiO_{4+x} with $x > 0.05$ (*42*). The c-axis internal electric field apparently lowers the antibonding $(O_2)^{2-}$ level below the Fermi energy E_F in the CuO_2 sheets. Introduction of the interstitial oxide ion reduces the tensile stress on the rocksalt layer, and oxidation of the CuO_2 sheets reduces the compressive stress on these sheets.

As prepared under 1 atm O_2, La_2CuO_{4+x} consists primarily of the $x < 0.02$ phase, which is not a superconductor, but some $x > 0.05$ phase may appear at the grain boundaries to give filamentary superconductivity. Preparation under 3 kbar O_2 atm (*6*) yields two-phase material with a large fraction of the bulk being the superconductor phase

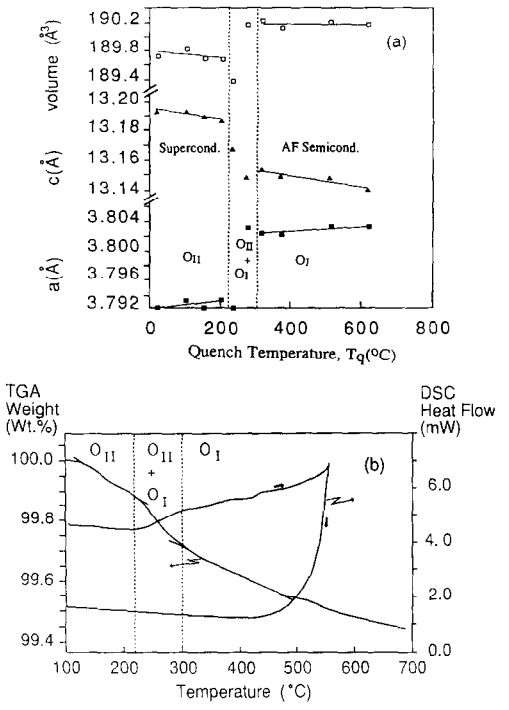

FIG. 7. (a) Variation of room temperature lattice parameters and volume with quench temperature T_q for La_2CuO_{4+x} heated successively to higher T_q and (b) TGA and DSC curves in N_2 atom at 1°C/min of La_2CuO_{4+x}.

with $x > 0.05$; preparation at 23 kbar O_2 atm (*7*) results in a bulk superconductor with $x \geq 0.05$. Thermogravimetric analysis (TGA) and Differential Scanning Calorimetry (DSC) of the $La_2CuO_{4.05}$ phase obtained at 23 kbar O_2 atm shows an abrupt loss of oxygen and a first-order phase change in the interval $225 < T < 275$°C (Fig. 7) (*7*). Figure 7 also shows the variation with quench temperature T_q of the room temperature lattice parameters for a sample of $La_2CuO_{4.05}$ raised successively to higher T_q in air before quenching to room temperature for X-ray diffraction. A remarkable increase in 1/2 (a + b) on passing from the superconductor to the antiferromagnetic phase with loss of oxygen is consistent with an important suppression of the atomic moment on the Cu in the superconductive state. Such lattice dilatations on passing from the superconductor to the antiferromagnetic phase have also been noted for the other copper oxide systems (*43*). A first-order phase change associated with the change in mobile-hole concentration is consistent with the postulate (*2*) of charge fluctuations in the superconductor phase that distinguish "bags" in which superconductive pairs are formed from normal-state regions supporting spin fluctuations.

E. The Systems $Ln_{2-y}Ce_yCuO_4$, Ln = Pr, . . . Gd

Replacement of a larger Ln^{3+} ion by a smaller Ce^{4+} ion in the T′ phases not only relieves the compressive stress in the Ln–O_2–Ln layer; it also reduces the tensile stress in the CuO_2 sheets by donating to the sheets an antibonding $\sigma^*_{x^2-y^2}$ electron, which occupies the upper Hubbard band. Reduction of the copper coordination from six to four as well as the change from a compressive to a tensile stress on the CuO_2 sheets lowers the upper Hubbard band in the T′ phase relative to its position in the T phase. In fact, the Fermi energy of the n-type T′ phase is about the same as that of the p-type T phase (*44*) despite the fact that optical data of Suzuki (*45*) place the upper Hubbard band about 2 eV above the filled band (π^* or lower Hubbard $\sigma^*_{x^2-y^2}$) in La_2CuO_4.

The phase diagram for the system $Nd_{2-y}Ce_yCuO_4$ is shown in Fig. 8. The Néel temperature as determined by muon spin rotation (μSR) (*46*) decreases much more slowly with Ce doping in this system than does T_N with Sr doping in p-type $La_{2-y}Sr_yCuO_4$. An abrupt drop in T_N around $y \approx 0.13$ occurs at the transition, with increasing y, to the superconductor phase. In the superconductor phase, T_c decreases with increasing y from a maximum of 20 K around $y = 0.15$ until it vanishes at $y \approx 0.18$. As in the p-type system, the transition from a superconductor to a normal metal is accompanied by a

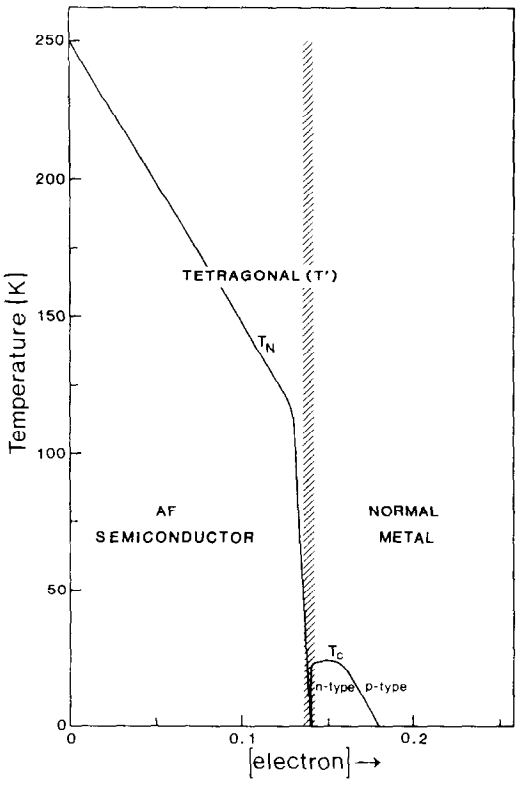

FIG. 8. Phase diagram for the system $Nd_{2+x}Ce_xCuO_4$ (adapted from Ref. (*46*)).

change in the sign of the charge carrier (*25*). Thus the *n*-type superconductors exhibit the same confluence of special features as the *p*-type superconductors; however, the rate of increase of W with increasing electron concentration does not appear to be so dramatic, as indeed must be expected for a $W \sim \varepsilon_\sigma(\lambda_\sigma^2 + \lambda_s^2)$.

Although $Gd_{2-y}Ce_yCuO_4$ could be obtained as a single-phase material up to $y \approx 0.15$, no superconductivity has been observed in this system. A smaller a-parameter for Ln = Gd compared to Ln = Nd increases the strength of the Cu–O interactions in the CuO_2 sheets, which must raise the upper Hubbard band of antibonding $\sigma^*_{x^2-y^2}$ orbitals relative to the $Ce^{3+}: 4f^1$ energy level. The smaller the energy separation between the $Ce^{3+}: 4f^1$ energy level and the Fermi energy E_F, the greater is the hybridization of Ce–4*f* and $\sigma^*_{x^2-y^2}$ band states. A hybridization of narrow-band and localized 4*f* states can, if strong enough, transform the narrow-band states to small-polaron states, thereby suppressing superconductivity.

Support for a $Ce: 4f^1$ energy close to the Fermi energy E_F in $Gd_{2-y}Ce_yCuO_4$ comes from the following observations: The lower limit for the mean Ln^{3+} ionic radius in the T′ phase is realized at $y \approx 0.6$ in $Gd_{2-y}Dy_yCuO_4$; for $y > 0.6$, impurity phases appear. However, the y value can be increased to $y = 0.9$ if about 0.1 Ce is present as in $GdDy_{0.9}Ce_{0.1}CuO_4$. Since the addition of Ce as Ce^{4+} would add antibonding electrons to the CuO_2 sheets, thereby increasing the bond-length mismatch between fluorite and CuO_2 layers at the stability limit of the phase, it is concluded that the Ce must be present as Ce^{3+} ions to stabilize the T′ phase. If all the Ce is present as Ce^{3+}, the mean Ln^{3+} ionic radius (for eight-fold coordination) becomes 1.0458 Å, which is close to that in $Gd_{1.4}Dy_{0.6}CuO_4$ (1.0452 Å).

The solubility range of Ce in $Ln_{2-y}Ce_yCuO_4$ increases with increasing mean size of the lanthanide ion in the fluorite layer. For example, single phases are found for $y \leq 0.25$, 0.20, and 0.15 for $Ln = La_{0.65}Nd_{0.35}$, Nd, and Gd, respectively. The increasing tensile stress on the CuO_2 sheets with increasing mean lanthanide ion size appears to control the solubility range of Ce. By substituting Ce for Nd with $Ln = La_{0.65}Nd_{0.35}$ in the system $La_{1.3}Nd_{0.7-y}Ce_yCuO_4$, it is possible to extend the range of electron doping well into the normal-metal phase of Fig. 8.

The introduction of interstitial oxygen into the system $La_{1.3}Nd_{0.45}Ce_{0.25}CuO_{4+x}$ has interesting consequences for the electronic properties. Firing at 1060°C followed by an anneal in 1 atm O_2 at 400°C gives a semiconductor composition with $x = 0.04$ (Fig. 9a),

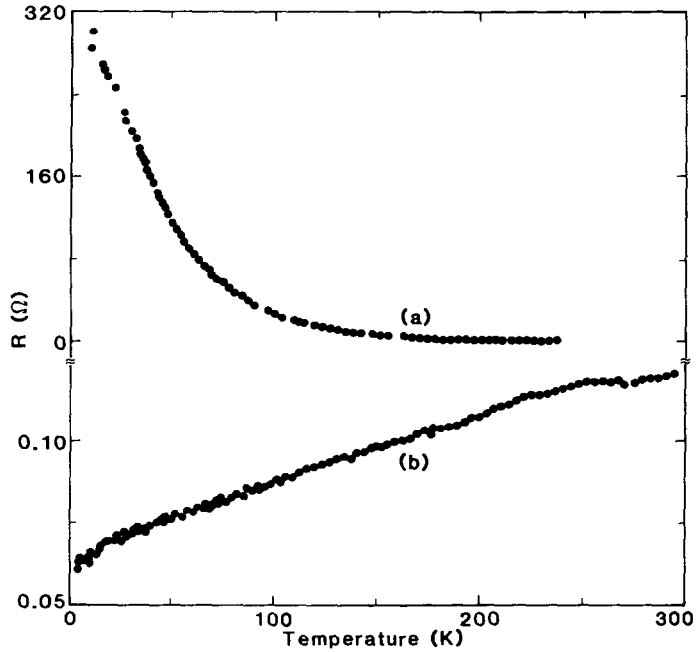

FIG. 9. Resistivity vs temperature for $La_{1.3}Nd_{0.45}Ce_{0.25}CuO_{4+x}$: (a) $x = 0.04$ and (b) $x = 0.0$.

even though an electron concentration $n = 0.17$ per formula unit in the CuO_2 sheets is calculated for this composition (*47*). Annealing in N_2 at 900°C gives $x = 0.0$ and a normal-metal behavior (Fig. 9b), consistent with the higher electron concentration $n = 0.25$ according to the phase diagram of Fig. 8. It is apparent that the excess 0.04 oxygen atoms, which can only occupy *c*-axis positions, perturb the conduction band sufficiently to introduce Anderson-localized states at the edges of the narrow $\sigma^*_{x^2-y^2}$ bands. This type of charge-carrier trapping within band tails leads to a conductivity described by variable-range hopping (*48*). Because the bands are at the narrow-band limit, relatively small perturbations can introduce Anderson localization.

III. Oxygen and the $YBa_2Cu_3O_{6+x}$ Structure

The tetragonal $YBa_2Cu_3O_6$ and orthorhombic $YBa_2Cu_3O_7$ structures are shown in Fig. 10; they consist of the intergrowth sequence along the *c*-axis

$$|CuO_2\text{–}Y\text{–}CuO_2|BaO\text{–}CuO_x\text{–}BaO| \quad (7)$$

in which the superconductively active layers contain two CuO_2 sheets and the inactive layers have a variable oxygen content x in the formulation $YBa_2Cu_3O_{6+x}$. The number of oxygen sites in a CuO_x plane is two per formula unit, so the oxygen content can vary over the range $0 \leq x \leq 2$ from a stereochemical point of view; in fact, the upper limit of x under 1 atm of O_2 in $YBa_2Cu_3O_{6+x}$ appears to be about 0.96 with an ordering of the oxygen into *b*-axis sites of the orthorhombic structure.

As in the La_2CuO_4 structure, the interface between the two intergrowth layers requires bond-length matching between a CuO_2 sheet and an (001) rocksalt plane, which is here a BaO rather than an LaO plane. Therefore it would appear that the tolerance factor of Eq. (3) should apply in this structure also.

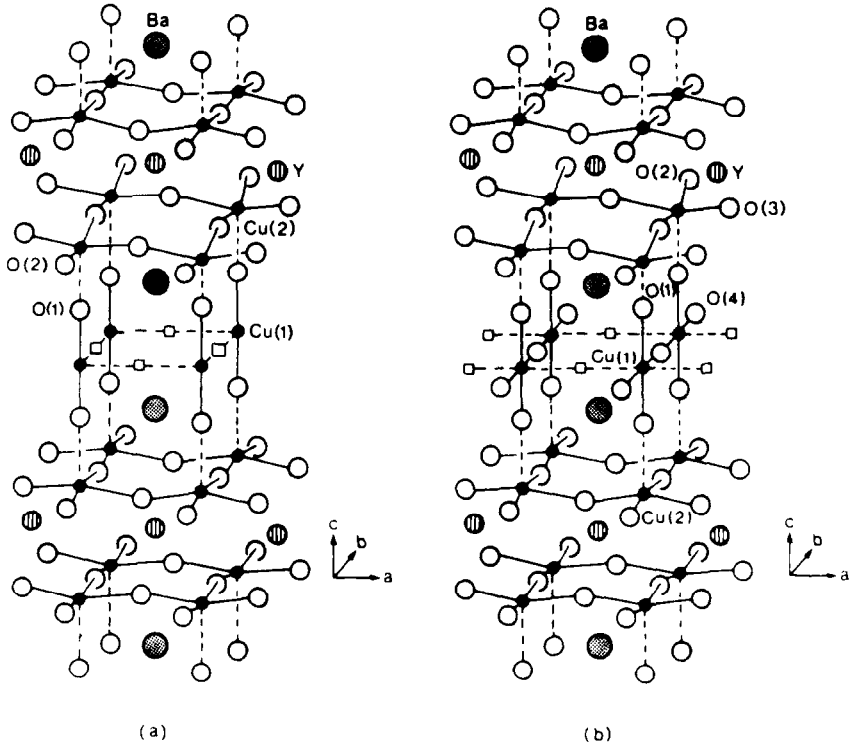

FIG. 10. Structures for (a) tetragonal $YBa_2Cu_3O_6$ and (b) ideal, orthorhombic $YBa_2Cu_3O_7$.

However, the Cu–O–Cu bonds are bent from 180° by the fact that the O atoms of a CuO_2 sheet interact with Y^{3+} ions on one side and Ba^{2+} ions on the other. In addition, the Ba–O–Ba bonds are bent from 180° because the *c*-axis oxygen bond to a fivefold-coordinated Cu in the CuO_2 sheets and a twofold-coordinated Cu in the Cu plane for $x = 0$; in $YBa_2Cu_3O_6$, the *c*-axis oxygen are closer to the Cu(1) atoms in the Cu plane than to the Cu(2) atoms of a CuO_2 sheet. The structurally adjustable parameter in this structure type appears to be a *c*-axis displacement of the equilibrium position of the oxygen atoms rather than a tilting of the CuO_5 square pyramids of a CuO_2 sheet (*47*). As x increases, the *c*-axis oxygen move away from the Cu(1) toward the Cu(2) atoms (*49*), and the *c*-axis Cu(2)–O distance appears to modulate the width W of the conduction band (*47*).

In this latter connection, it is instructive to examine the system $Nd_{2-z}Ce_zBa_{2-y}La_yCu_3O_{8+x}$, which has a structure similar to that of $YBa_2Cu_3O_{6+x}$ except for the substitution of a fluorite layer for the Y plane in the superconductively active layer (*50, 51*):

$$|CuO_2\text{–Nd, Ce–}O_2\text{–Nd, Ce–}CuO_2|(Ba, La)O\text{–}CuO_x\text{–}(Ba, La)O|. \quad (8)$$

This system exhibits an orthorhombic distortion above a critical value of y, but the distortion is not due to either a tilting of the CuO_5 square pyramids or an ordering of the oxygen into *b*-axis sites in the CuO_x plane; it appears to reflect an ordering of the cations and a cooperative *c*-axis oxygen displacement in the (Ba, La)O rocksalt planes (*47*).

Of particular interest in $Ba_2Cu_3O_{6+x}$ is the

variability x of the oxygen content and the role of the oxygen coordination at the Cu atoms in controlling the distribution of the formal oxidation state at the copper atoms. Where the Cu are linearly coordinated by two oxygen atoms, as in the Cu(1) planes of the $YBa_2Cu_3O_6$ structure, the copper have the formal valence Cu^+. Where the copper are coordinated by five oxygen, as in the $Cu(2)O_2$ planes, the copper may have the formal valence $Cu^{(2+p)+}$, where $p = 0$ in $YBa_2Cu_3O_6$ and $p = 0.5$ in the ideal $YBa_2Cu_3O_7$ structure of Fig. 10b. In this ideal $YBa_2Cu_3O_7$ structure, the Cu(1) atoms are all coordinated by four coplanar oxygen atoms—a cooperative tilting of the coplanar arrays about the c-axis bends the Cu(1)–O–Cu(1) bond angle of a b-axis chain from 180° (*52*); the four-coordinated Cu(1) atoms have the formal valence Cu^{2+}. With seven oxygen per formula unit, the successive layers are uncharged, which eliminates any c-axis electric field, and the valence distribution is determined by the different crystalline fields at the copper with fivefold versus fourfold coordination.

This observation makes it of interest to explore the variation in valency distribution as a function of x in the system $YBa_2Cu_3O_{6+x}$ with and without ordering of the oxygen in the CuO_x plane.

The oxygen of a CuO_x plane retain their maximum order if removed at low temperature from a sample of initial composition $YBa_2Cu_3O_{6.96}$. The oxygen atoms of the $Cu(1)O_x$ planes become mobile above 300°C (*53*). It is therefore feasible to remove oxygen progressively in the temperature interval $300 < T \leq 900$°C; this has been done by making use of either a Zr-gauze oxygen getter (*54*) or a stabilized-zirconia oxygen pump (*55*). Alternatively, use can be made of a plot of sample weight versus temperature in air to determine the value of x at a particular temperature; x varies from 0.96 at 300°C to close to zero at the temperature of synthesis (~920°C). By quenching to room

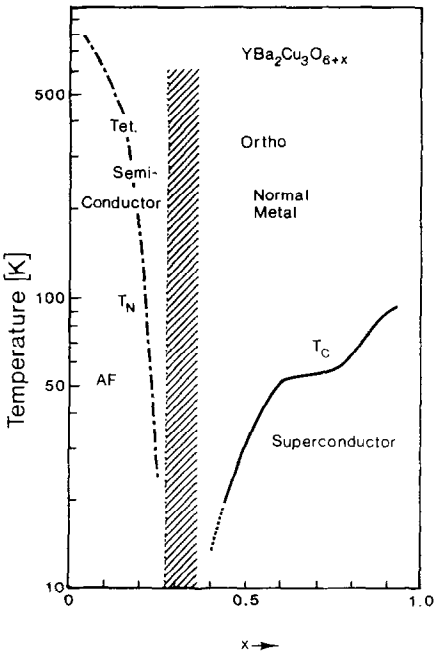

FIG. 11. Phase diagram for the system $YBa_2Cu_3O_{6+x}$.

temperature, it is possible to vary x over the range $0 \leq x \leq 0.96$; and a subsequent anneal in vacuum or an inert atmosphere below 400°C allows ordering of the oxygen to take place (*56*). Such experiments result in a step-like T_c vs x variation like that shown in Fig. 11. Although the literature remains controversial on the interpretation of this curve, it can be understood in a straightforward manner in terms of oxygen ordering and a cation valence determined by the oxygen coordination (*56, 57*). In addition, the interpretation requires a T_c proportional to the concentration of mobile holes p in the CuO_2 sheets; but this relationship has been established by μSR measurements (*58*), which have for the $YBa_2Cu_3O_{6+x}$ system with $x \leq 0.9$, a

$$T_c \sim p/m^*, \tag{9}$$

where the variation of the effective mass m^* with p can probably be ignored in a zero-order consideration of the problem.

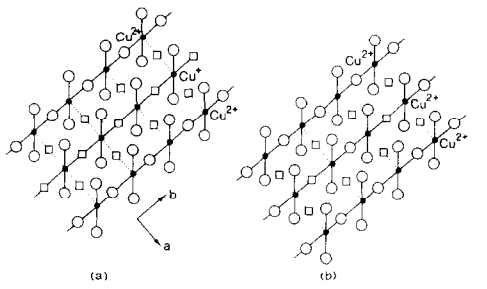

FIG. 12. Ideal oxygen ordering in $YBa_2Cu_3O_{6+x}$ for (a) $x = 0.5$ and (b) $x = 0.75$.

The first level of ordering among the oxygen of a $Cu(1)O_x$ plane is found for $x = 1$; the oxygen atoms occupy the b-axis within the $Cu(1)O_x$ plane (Fig. 10b). A second level of ordering at $x = 0.5$ has been identified by electron microscopy (*59*); it consists of alternate b-axis chains of fourfold-coordinated and twofold-coordinated Cu(1) atoms. With perfect order, the two types of Cu(1) atoms would have, respectively, the formal valencies Cu^{2+} and Cu^{+}, so the total oxidation state would then imply a concentration $p = 0.25$ of mobile holes per $Cu(2)O_2$ sheet. The $x = 0.5$ composition is, therefore, a superconductor with a T_c that varies with the degree of order in the $Cu(1)O_x$ planes.

The fact that no mobile holes are introduced into the CuO_2 sheets in the interval $0 \leq x \leq 0.25$ indicates that the initial insertion of an oxygen atom, which changes the coordination of its two neighboring Cu(1) atoms from twofold to threefold, results in the oxidation of the neighboring threefold-coordinated Cu(1) atoms from Cu^{+} to Cu^{2+}. Oxidation of the Cu(1) atoms does not introduce holes that are mobile at low temperature; these oxidations do not contribute to superconductivity. For $x > 0.25$, electrostatic O^{2-}–O^{2-} interactions within a CuO_x plane introduce an ordering of the oxygen into alternate b-axis chains (Fig. 12a), which changes the crystal symmetry from tetragonal to orthorhombic and results in the onset of oxidation of the CuO_2 sheets due to a preservation of half the Cu(1) as Cu^{+} ions.

In the interval $0.5 < x < 0.75$, oxygen atoms are introduced into the empty b-axis chains to make them partially occupied. At $x = 0.75$, an ordering within the partially occupied chains would leave each Cu(1) of the chain threefold-coordinated with a formal valence Cu^{2+} (see Fig. 12b), and no additional oxidation of the CuO_2 sheets would have occurred in the compositional range $0.5 < x < 0.75$ under conditions of perfect order. Although it is difficult to establish the type of ideal ordering predicted for $x = 0.75$, electron diffraction has shown additional diffraction spots at $(h^*/2,0,0)$ and $(0,k^*/2,0)$ in one untwinned crystal of composition $x \approx 0.75$ (*56*). For $x > 0.75$, all the Cu(1) are oxidized to Cu^{2+} and, with a primary ordering that retains fourfold or threefold coordination at each Cu(1) atom, the oxidation power in excess of Cu^{2+} for the Cu(1) atoms appears as an increase in the concentration p of mobile charge carriers in the CuO_2 sheets. Therefore T_c increases with x for $x \gtrsim 0.75$, but it apparently approaches saturation for $x > 0.9$. This approach to saturation would be analogous to the saturation that occurs near $y = 0.15$ in the system $La_{2-y}Sr_yCuO_4$ (see Fig. 5). Lack of complete oxygen ordering and homogeneity prevents the T_c versus x curve of Fig. 11 from exhibiting a flat plateau in the range $0.5 \leq x \leq 0.75$; in fact, the flatness of the step is very much a function of the heat treatment of the sample.

This explanation of the T_c vs x curve of Fig. 11 raises the question of the mechanism of oxygen insertion down a b-axis chain. Two routes are possible; one involves migration via an a-axis site, which would introduce a disorder that would create fivefold coordinated Cu(1) atoms that might become oxidized to Cu^{3+}. Alternatively, a correlated diffusion involving a cooperative displacement of c-axis oxygen to b-axis sites and b-axis oxygen to c-axis sites would per-

mit diffusion down a chain without occupancy of the *a*-axis sites. Isotope-exchange experiments (*60, 61*) and the loss of *c*-axis oxygen at higher temperatures (*62*) have established that the correlated diffusion mechanism is dominant and that the *c*-axis oxygen play an important role in the mobile-oxygen diffusion as well as in stabilizing different valence states via an adjustment of their *c*-axis position (*47, 49*).

A disordering of oxygen to *a*-axis sites of the $Cu(1)O_x$ planes may cause a trapping of holes as $Cu(1)^{3+}$ where such a disorder creates fivefold coordinated Cu(1) atoms. This fact has been established by two types of experiments. First, materials prepared at low temperatures from precursors may result in a disordered array of oxygen in the CuO_x planes with an $x > 0.5$. Second, substitution of Ba^{2+} by La^{3+} ions may introduce excess oxygen, $x > 1.0$, in the CuO_x planes.

We encountered the first situation on preparing $YBa_2Cu_3O_{6+x}$ from oxalate precursors at 780°C in order to obtain particles of submicron size (*63*). Although the oxygen content corresponded to $x = 0.7$, the particles were tetragonal—indicating disordered oxygen in the CuO_x planes—and semiconductive, not superconductive. Moreover, in air the variation in oxygen content below 780°C was much smaller compared to that in orthorhombic $YBa_2Cu_3O_{6+x}$; there appeared to be a lower oxygen mobility in the CuO_x planes in air until temperatures in excess of 800°C were used (*3*). Although it was possible to convert the tetragonal, semiconductive particles into orthorhombic, superconductive particles by heating above 800°C and then annealing in air at 400°C, sintering occurred at the higher temperatures.

These data indicate that mobile holes are trapped out of the CuO_2 sheets at fivefold-coordinated Cu(1) atoms in the CuO_x planes. This trapping is associated with the formation of an immobile complex, and X-ray photoelectron spectroscopy (XPS) showed shifts in the O: 1*s* core peaks characteristic of an important O–2*p* character in the hole-trapping orbitals (*64*). Although the simplest complex would be an $(O_2)^{2-}$ peroxide ion, no direct evidence for peroxide formation has been forthcoming. The XPS data may simply indicate the formation of a CuO_5 complex with an important O–2*p* component in the "Cu^{3+}" valence state due to the existence of an equilibrium reaction (Eq. (1)) that is biased more to the right than to the left.

The eventual preparation of submicron superconductor particles was successfully accomplished (*63*) by annealing in N_2 at 750°C; in this atmosphere the oxygen of the CuO_x planes are mobile at 750°C and can be removed; a subsequent anneal in air or 1 atm O_2 at 400°C reintroduces the oxygen in an ordered manner, and the particles—kept below 1 μm diameter—are transformed to an orthorhombic superconductor with $T_c \approx 90$ K.

A variety of ionic substitutions in $YBa_2Cu_3O_{6+x}$ have been carried out in an attempt to probe further the structure–property relationships in this phase. These studies have established four general findings concerning substitutions for Y and Ba:

—All isovalent and aliovalent substitutions in the Y or Ba sites leave the equilibrium oxidation of the Cu–O array unchanged over wide solid-solution ranges; with an anneal at 400°C in 1 atm O_2, this oxidation state generally corresponds to an $x = 0.95 \pm 0.01$ in $YBa_2Cu_3O_{6+x}$ except for the case $YBa_{2-y}La_yCu_3O_{6+x}$ where, for $y \geq 0.1$, it extrapolated to $x = 0.90 \pm 0.02$ for $YBa_2Cu_3O_{6+x}$ (*65–68*).

—With the exception of Pr substitution for Y (discussed in Section IV), the critical temperature T_c varies with the mobile-hole concentration p in the CuO_2 sheets in approximate accordance with Eq. (9) (*58, 67*).

—Replacement of a Ba^{2+} ion by a Ln^{3+} ion introduces near-neighbor oxygen at *a*-axis sites of the adjacent CuO_x planes, which

lowers the macroscopic orthorhombicity of the structure.

—Beyond a critical concentration of *a*-axis oxygen in the CuO_x planes, two mobile holes per excess *a*-axis oxygen are trapped out of the CuO_2 sheets, and the critical concentration changes with the strength of the internal *c*-axis electric field (*66–68*).

Consider, for example, the system $YBa_{2-y}La_yCu_3O_{6+x}$ for which $x \approx 0.90 + 0.5y$ and

$$T_c \approx 90 - 200(y - 0.15) = (120 - 200y)\text{K} \quad (10)$$

for $0.1 \leq y < 0.5$. (A $y - 0.15$ is used in Eq. (10) because of the extrapolation to $x = 0.90$ at $y = 0$.) At $x = 0.90$ in $YBa_2Cu_3O_{6+x}$, a $T_c \approx 90$ K corresponds to 0.45 holes per CuO_2 sheet per formula unit, so Eq. (10) with Eq. (9) would correspond to the trapping out of two mobile holes from the CuO_2 sheets per oxygen in excess of the critical value $x_c = 0.95$ found at $y = 0.1$. Hall measurements for the system $NdBa_{2-y}Nd_yCu_3O_{6+x}$, which has a similar variation of T_c with y, have provided direct evidence of a trapping from the CuO_2 sheets of two mobile holes per excess oxygen atom introduced by a $y > 0.1$ (*69, 70*). The observation of a trapping of two holes per interstitial oxygen in excess of $x = 0.96$ was at first thought (*66*) to confirm the formation of an oxygen cluster like the peroxide ion $(O_2)^{2-}$, which was originally postulated to occur in the disordered CuO_x planes obtained by low-temperature decomposition of the oxalates (*63*), especially as similar splittings of the O: 1*s* XPS spectra were observed (*64*). However, it now appears more likely that two mobile holes per *a*-site oxygen are trapped out from the CuO_2 sheets at two fivefold-coordinated Cu(1) sites created by an *a*-axis oxygen where there is an $x > 0.95$. Clearly the trapping energy must increase the higher the negative charge of the CuO_x planes. Trapping out of the mobile holes can occur only

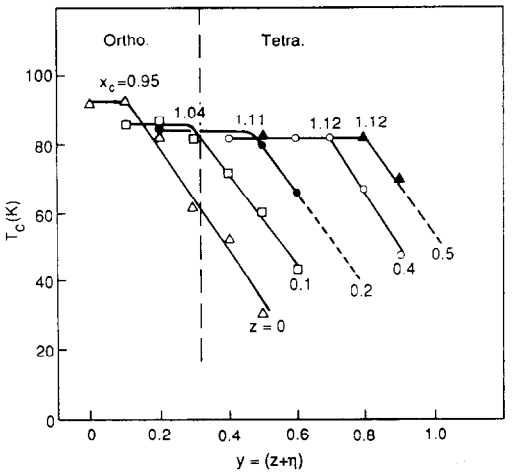

FIG. 13. Variation of T_c with $y = z + \eta$ for various values of z in the system $Y_{1-z}Ca_zBa_{2-y}La_yCu_3O_{6+x}$ annealed in 1 atm O_2 at 400°C; x_c refers to the critical oxygen content at which hole trapping occurs.

for oxygen in excess of a critical value; trapping of the holes effectively neutralizes the potential change introduced by an additional *a*-axis oxygen. Moreover, the critical value x_c at which holes become trapped should increase with a decrease in the positive charge of the Y^{3+} plane. Indeed, substitutions of Ca^{2+} for Y^{3+} in the codoped system $Y_{1-z}Ca_zBa_{2-y}La_yCu_3O_{6+x}$ (*67, 68*) tends to increase the value of x_c above which trapping out of the mobile holes occurs, as can be seen from the plots in Fig. 13 of T_c vs y for different values of z. We have also been able to show, from thermoelectric-power measurements (*37*), that the depth of the two-hole traps increase with increasing y for a given value of z.

Figure 13 also shows that the transition from orthorhombic to tetragonal macroscopic symmetry occurs at roughly the same value of y for all systems, which is compatible with a location of *a*-axis oxygen as near neighbors to the La^{3+} ions. Moreover, for each value of z the T_c vs y curve shows no change on passing through the orthorhom-

bic–tetragonal transition. It is clear that what determines the magnitude of T_c is the concentration of mobile holes in the CuO_2 sheets and not the macroscopic symmetry of the crystallites.

IV. Problems with Pr

The $YBa_2Cu_3O_{6+x}$ structure does not tolerate the substitution of a quadrivalent ion such as Ce^{4+} for the Y^{3+} ion; however, all the Ln^{3+} ions are readily substituted (*71*). With the exception of Ln = Pr, the existence of a localized $4f^n$ spin configuration on the rare earth ion has little influence on T_c, which shows that there is little interaction between the $4f^n$ configuration and the $\sigma^*_{x^2-y^2}$ band states of the CuO_2 sheets near the Fermi energy E_F. On the other hand, T_c decreases rapidly with increasing z in the system $Y_{1-z}Pr_zBa_2Cu_3O_{6+x}$, which immediately led to the suggestion that at least some of the Pr are present as Pr^{4+} ions (*72*). However, photoemission (*73*), XANES (*74*), and X-ray absorption (*75*) data have all indicated that the Pr valence remains Pr^{3+}. Transport measurements (*76*) have indicated a transition from itinerant-electron conduction to either small-polaron or variable-range-hopping conduction with increasing z in $Y_{1-z}Pr_zBa_2Cu_3O_{6+x}$; Neumeier *et al.* (*77*) provided convincing evidence from the pressure dependence of T_c for a strong hybridization of Pr–4*f* and O–2*p* orbitals without a change in the valence state Pr^{3+}. All these results point to a $Pr^{3+}:4f^2$ level E_f that lies below E_F, but by a small energy $\Delta_f = (E_F - E_f)$. A small Δ_f allows an important hybridization of the Pr–4*f* and $\sigma^*_{x^2-y^2}$ orbitals via a covalent-mixing parameter $\lambda_f = b_f/\Delta_f$ even though the matrix element b_f containing the overlap of crystal-field $\sigma^*_{x^2-y^2}$ and Pr–4*f* orbitals is small. Since Eq. (9) holds and the density of one-electron states in a two-dimensional $\sigma^*_{x^2-y^2}$ band is constant, it follows that if the number of holes in the CuO_2 sheets remains constant, the number of mobile holes must decrease with increasing z. We therefore conclude that the hybridization of localized Pr–4*f* orbitals with $\sigma^*_{x^2-y^2}$ band states perturbs the bands so as to create Anderson-localized states at the edges of the $\sigma^*_{x^2-y^2}$ band; this localization of band states reduces the density of mobile-hole states below the mobility edge, and superconductivity disappears where the mobility edge crosses the Fermi energy with increasing z.

If this analysis is correct, then changes in the crystalline fields that increase Δ_f should eliminate the suppression of T_c by Pr substitutions. To explore this possibility, the influence of Pr substitution was investigated for several different systems (*78*). We found that the introduction of Pr into $La_{1.85-y}Pr_ySr_{0.15}CuO_4$, which has the T/O structure of La_2CuO_4, and into $Bi_2Sr_{2-2y}Pr_{2y}CuO_6$ and $Bi_2Sr_2Ca_{1-z}Pr_zCu_2O_{8+x}$, has no more influence on T_c than do other Ln^{3+} ions such as Ln = Nd or La. On the other hand, substitution of Pr for La in the T* structure of $Ln_{2-y-z}Ce_ySr_zCuO_4$ decreases T_c (*79*) in a manner similar to its influence in $Y_{1-z}Pr_zBa_2Cu_3O_{6+x}$. Figure 14 shows the formal charge on traversing the *c*-axis. If the sum of the formal positive charge per formula unit on the two planes adjacent to a CuO_2 sheet is $Q \geq +3e_0$, where e_0 is the magnitude of the electronic charge, then Pr^{3+} ions in one of those planes suppress T_c; they do not do so for a $Q \leq 2e_0$. The larger the value of Q, the higher the Madelung energy shifts E_f relative to the E_F of the $\sigma^*_{x^2-y^2}$ bands of an adjacent, negatively charged layer. Therefore a larger Q means a smaller Δ_f and hence a greater perturbation of the $\sigma^*_{x^2-y^2}$ band by hybridization with the $Pr^{3+}:4f^2$ level.

Despite this evidence, Neumeier *et al* (*80*) have subsequently claimed to present evidence that the Fermi energy E_F intersects the $Pr^{4+/3+}$ couple for smaller values of η in the codoped system $(Y_{1-z-\eta}Pr_zCa_\eta)Ba_2Cu_3O_{6+x}$. However, their analysis was based on two assumptions that appear to be

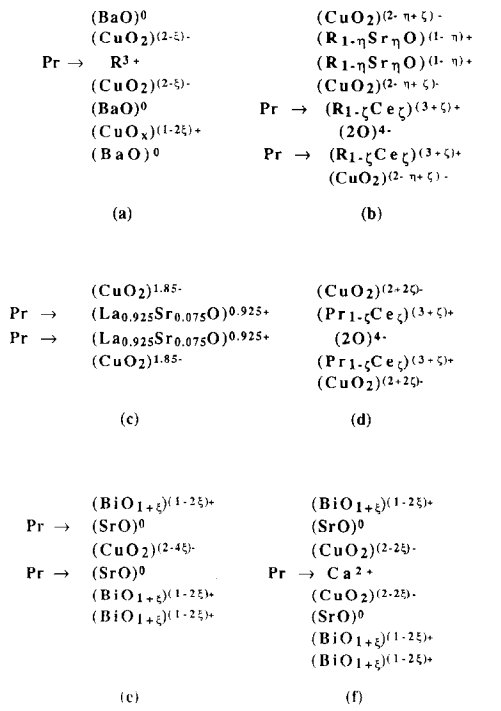

FIG. 14. The formal charge per formula unit for successive basal planes in the structures (a) $RBa_2Cu_3O_{6+x}$, (b) $R_{2-y-z}Ce_ySr_zCuO_4$, $y > Z(T^*)$, (c) $La_{1.85}Sr_{0.15}CuO_4$ (T), (d) $Pr_{2-z}Ce_zCuO_4$ (T'), (e) $Bi_2Sr_2CuO_{6+x}$, and (f) $Bi_2Sr_2CaCu_2O_{8+x}$. $\xi = 0.5x$, $\eta = 0.5z$, $\zeta = 0.5y$, and R = lanthanide or y.

incorrect: (i) the oxygen content remains constant at $x = 0.95 \pm 0.02$ for all values of η and (ii) the samples are essentially single-phase, any small amount of second phase being independent of η. Our data for this system (*81*) show that (i) the equilibrium oxidation of the system—not the oxygen content—remains constant and (ii) the concentration of impurity phases such as Ba CuO_2 increases with η if the samples are prepared in air at 930°C. However, the concentration of the impurity phases remain minimal and constant if the samples are prepared at 920°C in 1 atm O_2. Samples with $z = 0.2$ prepared in 1 atm O_2 at 920°C show a monotonic increase in T_c from 70 K at $\eta = 0$ to 78 K at $\eta = 0.2$ as could be expected for a lowering of Q in the Y^{3+} plane at a constant hole concentration in the $\sigma^*_{x^2-y^2}$ bands of the CuO_2 sheets. On the other hand, samples prepared in air at 930°C show an initial increase in T_c from 68 K at $\eta = 0$ to 73 K at $\eta = 0.05$ followed by a decrease to 66 K at $\eta = 0.2$, which is similar to the results reported by Neumeier *et al.* (*80*). These results clearly demonstrate that the complex variation of T_c with η reported by Neumeier *et al.* (*80*) is due to a varying concentration of impurity phases and not to an overlap of E_F with the $Pr^{4+/3+}$ redox couple.

V. Thallium and Bismuth Cuprates

The structures of the $TlBa_2Ca_{n-1}Cu_nO_{2n+3}$ and the $Tl_2Ba_2Ca_{n-1}Cu_nO_{2n+4}$ families are shown in Figs. 15 and 16. Phases with $n = 1$–5 have been identified (*82–90*). These structures may be visualized as an intergrowth of superconductively active $Ca_{n-1}(CuO_2)_n$ layers and inactive BaO–TlO–BaO (Fig. 15) or BaO–TlO–TlO–BaO (Fig. 16) layers. Since only the outer CuO_2 sheets of the active layers have five-fold-coordinated copper, we may anticipate that only these outer CuO_2 sheets of an active layer become oxidized and superconductive. This expectation finds support from the observed variation of the maximum T_c value with n, the number of CuO_2 sheets in an active layer. A maximum $T_c \approx 125$ K is found for $n = 3$; T_c decreases with increasing $n > 3$. For $n = 2$, a $T_c \approx 100$ K is obtained. Communication across one Ca–CuO_2–Ca layer is probably maintained, but it apparently decreases with increasing separation of the outer CuO_2 sheets of the active layer.

In these families also the interface between an active and an inactive layer consists of a CuO_2 sheet and an (001) rocksalt BaO plane; but the bond-length mismatch is alleviated by a bending of the Cu–O–Cu bonds from 180° because of stronger Cu–O

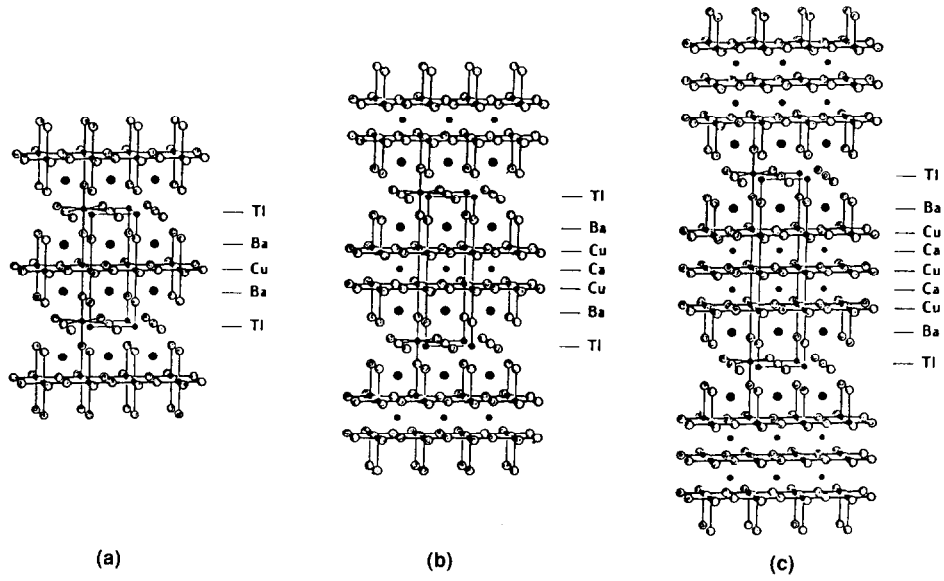

FIG. 15. Structures of (a) $TlBa_2CuO_5$, (b) $TlBa_2CaCu_2O_7$, and (c) $TlBa_2Ca_2Cu_3O_9$.

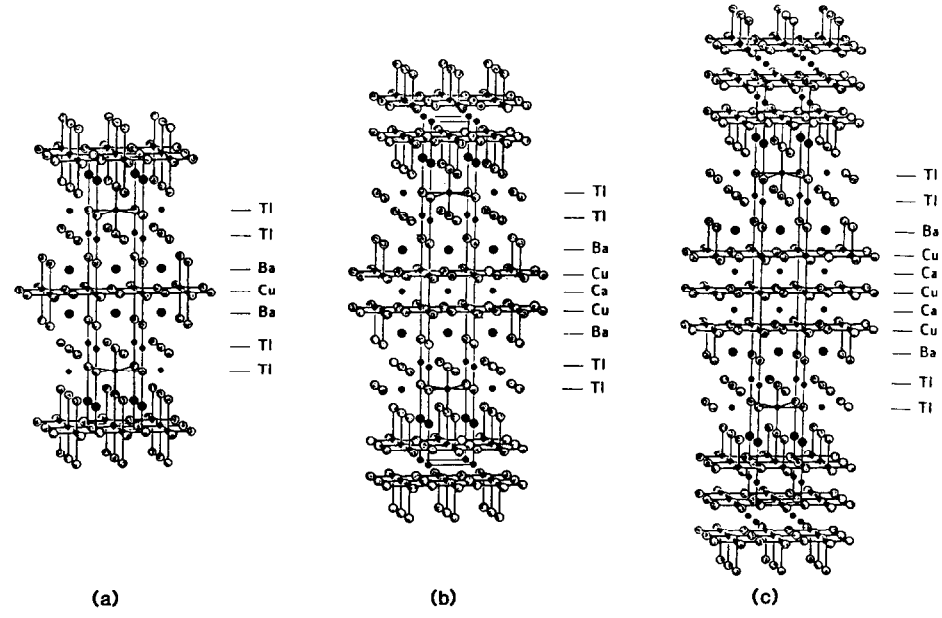

FIG. 16. Structures of (a) $Tl_2Ba_2CuO_6$, (b) $Tl_2Ba_2CaCu_2O_8$, and (c) $Tl_2Ba_2Ca_2Cu_3O_{10}$.

versus Ba–O bonding. A bending of the Ba–O–Ba bonds in a BaO plane also occurs.

The $Bi_2Sr_2Ca_{n-1}Cu_nO_{2n+4+x}$ family has an intergrowth structure similar to the Tl_2 family of Fig. 16, but with Bi substituted for Tl and Sr for Ba. However, there are important differences in the nominal TlO–TlO and BiO–BiO layers, as is discussed below. Although the $n = 1$ and 2 members of the Bi_2 family are readily synthesized, stabilization of the $n = 3$ member requires substitution of part of the Bi by Pb (*91*). A family having a single BiO layer is not known.

The Bi^{3+} ion differs from the Tl^{3+} ion by the presence of a $6s^2$ "lone pair"; the $6s^2$ energies at a Bi^{3+} ion are considerably more stable than the $6s^2$ energies at a Tl^+ ion. The lone pair on the Bi^{3+} ions appear to be polarized toward the neighboring BiO plane; these planes are stabilized in pairs within the bulk and are easily cleaved at the surface. The Tl_2 family is not easily cleaved.

In the Bi family, the Bi and O atoms are displaced considerably from their ideal positions to form "ladder-like" structures in the Bi_2O_2 layer (*92–94*). The displacements allow the insertion of rows of interstitial oxygen parallel to the *a*-axis that provide a long-wavelength modulation of the structure along the *b*-axis. From the easy cleavage of the Bi_2O_2 layers and the known chemistry of Bi^{3+} oxides, oxidation of the Bi^{3+} ions in preference to the CuO_2 sheets does not appear to occur. This deduction is supported by band calculations (*94*), which place the Bi : $6s^2$ energies below E_F and the Bi : 6p energies at least 1 eV above E_F. Since all the Bi remain Bi^{3+}, any oxidation of the CuO_2 sheets beyond the formal valence Cu^{2+} is generally accepted to be primarily due to the incorporation of excess oxygen in the Bi_2O_{2+x} layers (*93–96*); some contribution may also come from cation vacancies, which are revealed by microprobe analysis (*97*).

On the other hand, the origin of the oxidation of the CuO_2 sheets in the analogous Tl_2 family is quite different. However, the establishment of the primary mechanism has awaited the development of a satisfactory chemical procedure for determining both the thallium and oxygen contents of the final product (*98*). Without such a procedure, uncertainties in the Tl content arise from the volatility of Tl_2O during synthesis, and conventional iodometric determination of the oxygen content is blocked as bulk dissolution of the thallium cuprates in a mixture of KI and HCl is prevented by the formation of a passive coating, probably of iodides. In the absence of any analytical data, several sources of oxidation have been suggested: (i) the presence of Tl vacancies, which are revealed by microprobe analysis (*99, 100*), (ii) a mixed $Tl^{3+/+}$ valence in the Tl_2O_2 layer as revealed by XPS (*101–103*) and in accordance with band calculations (*104*) and/or (iii) excess oxygen in the Tl_2O_2 layer (*105, 106*) similar to that found for the Bi_2O_{2+x} family.

In recognition of the need for firm analytical data, we have adopted (*98*) both a simple wet-chemical procedure to determine the absolute Tl content (*107*) and a modified iodometric procedure to get the total oxygen content (*108*). Our analytical results for nominal "$Tl_2Ba_2CuO_6$" and "$Tl_2Ba_2CaCu_2O_8$"—obtained by firing initimate mixtures of the component oxides for 10 min in a premaintained muffle furnace at 900°C in air within a wrapped gold foil followed by quenching into liquid nitrogen—showed, respectively, a stoichiometry of $Tl_{1.92}Ba_2CuO_{5.59}$ and $Tl_{1.9}Ba_2CaCu_2O_{7.55}$ with a T_c = 63 and 90 K (*98*). If all the Tl are present as Tl^{3+}, then the observed stoichiometry gives a formal oxidation state much less than 2+ per Cu atom. On the other hand, these oxides show all the characteristics of *p*-type superconductors, which necessitates the oxidation of the CuO_2 sheets beyond the formal valence Cu^{2+}. The analysis rules out the presence of excess oxygen and it shows that the concentration of Tl vacancies is in-

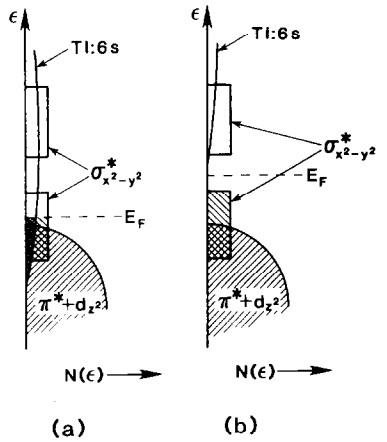

FIG. 17. Energy density of states $N(\varepsilon)$ vs energy ε for nominal (a) $Tl_2Ba_2CuO_6$ and (b) $TlBaLaCuO_5$.

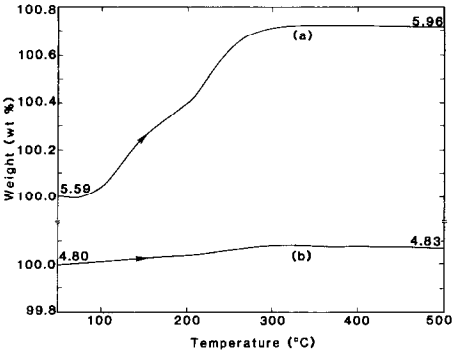

FIG. 18. TGA plots in 1 atm O_2 at 1°/min for (a) $Tl_{1.92}Ba_2CuO_{5.59}$ and (b) $Tl_{0.85}BaLaCuO_{4.8}$. The numbers refer to oxygen content. The Tl and oxygen contents were obtained from wet chemical analysis.

sufficient to dope the CuO_2 layers p-type. It follows that, in the Tl_2 family, there must be an overlap of the Tl–6s and $\sigma^*_{x^2-y^2}$ bands to induce an internal oxidation of the CuO_2 sheets and reduction of the Tl_2O_2 layers. This internal redox reaction appears to be dominant where there are few Tl vacancies. A schematic energy-band picture is given in Fig. 17a.

On the other hand, a nominal composition "$TlBaLaCuO_5$"—obtained by the above procedure—was found to have the composition $Tl_{0.85}BaLaCuO_{4.80}$ and to be a semiconductor (*109*). The absence of an oxidation of the CuO_2 sheets in this product clearly demonstrates that there is no overlap of E_F by the Tl–6s band in the family having a single Tl layer, as is indicated in Fig. 17b. This difference in the width of the Tl–6s band follows from a halving of the number of Tl–Tl nearest-neighbor interactions on going from the Tl_2 to the Tl family; it conforms to the band calculation (*104*).

Thermogravimetric analysis (TGA) obtained in O_2 at 1°/min up to 500°C (see Fig. 18) shows that $Tl_{0.85}BaLaCuO_{4.80}$ picks up only a negligible quantity of oxygen (0.03 oxygen per formula unit) whereas $Tl_{1.92}Ba_2CuO_{5.59}$ picks up about 0.37 oxygen per formula unit. Moreover, oxidation of the Tl_2 family is accompanied by an extrusion of approximately 0.3 Tl atoms per formula unit as Tl_2O_3—as obtained from X-ray intensity analysis—in the temperature range $70 < T < 350$°C whereas the Tl family does not extrude any Tl_2O_3 below 500°C. This remarkable difference is a direct consequence of the overlap of E_F by the Tl–6s band. Where the Fermi energy E_F intersects both the CuO_2–$\sigma^*_{x^2-y^2}$ and Tl–6s bands as in Fig. 17a, there the Tl–6s electrons are unstable relative to an oxidation reaction:

$$Tl^{(3-6\eta)+} + (3\eta/2)O_2 \rightarrow (1 - 2\eta)Tl^{3+} + \eta Tl_2O_3. \quad (11)$$

It is this mechanism that is the driving force for oxidation of the Tl_2 family. However, oxidation does not occur completely via an intercalation of excess oxygen into the Tl_2O_2 layers as in the Bi_2 family, but at least in part by a disintercalation of Tl or TlO. Tl is extruded from the Tl_2O_{2-x} layers until the bottom of the Tl : 6s band moves above E_F. Increasing the concentration of Tl vacancies decreases the number of Tl–Tl nearest-neighbor interactions, which narrows the Tl–6s band and thereby raises its bottom edge (*109*).

It follows immediately from these results that it should be possible to synthesize a more stable $Tl_{2-y}Ba_2CuO_{6-x}$ compound having a y large enough to maintain all Tl as Tl^{3+}. We have demonstrated (*109*) this to be true with a sample having $y \approx 0.5$.

VI. Conclusions

All the known copper oxide superconductors have intergrowth structures consisting of superconductively active CuO_2 sheets and other inactive layers. Crystal chemistry plays a key role in determining the type of doping—hole vs electron—and in modulating the superconductive properties. This paper has brought out the importance of the following aspects of the crystal chemistry.

(1) Stabilization of the intergrowth structures requires bond-length matching across the intergrowth interface. Investigation of the simplest system $La_{2-y}Ln_yCuO_4$ (*Ln* = lanthanide) has led to the identification of at least four different phases T/O, T′, T*, and T″ depending upon the size of *Ln* and the value of y. The T* structure has an interlayer ordering of T and T′ slabs whereas the T″ structure appears to have an intralayer ordering of cations and possibly anion displacements.

(2) The positive and negative charges of the intergrowths alternating along the c-axis creates an interlayer internal electric field parallel to the c-axis that can shift the energies within one layer relative to the other. The internal electric field modulates the distribution of holes between active and inactive layers—for example, in the codoped $Y_{1-z}Ca_zBa_{2-y}La_yCu_3O_{6+x}$ system—and controls the superconductive properties. It also influences the positioning of the Pr : $4f^1$ level relative to the Fermi energy and determines the influence of Pr on superconductivity.

(3) Copper atoms can exhibit a wide range of oxygen coordination numbers—from 2 to 6, which controls the distribution of the formal oxidation states at the copper atoms in complex systems such as $YBa_2Cu_3O_{6+x}$. The stereochemistry associated with different oxidation states of Cu appears to stabilize a number of ordered phases with interlayer and/or intralayer ordering of oxygen, which makes the variation of T_c with x complex in $YBa_2Cu_3O_{6+x}$.

(4) Oxidation/reduction of the CuO_2 sheets above/below the formal valence Cu^{2+} is one of the necessary conditions to induce superconductivity. Mixed valency can be created by (a) suitable ionic substitutions in the inactive layer as in $La_{2-y}Sr_yCuO_4$, $Nd_{2-y}Ce_yCuO_4$, and $Nd_2CuO_{4-x}F_x$, (b) intercalation of excess x oxygen in the inactive layer as in La_2CuO_{4+x}, $YBa_2Cu_3O_{6+x}$, and $Bi_2Sr_2Ca_{n-1}Cu_nO_{2n+4+x}$, (c) internal redox reaction, i.e., overlapping of two interlayer bands as in $Tl_{2-y}Ba_2Ca_{n-1}Cu_nO_{2n+4-x}$ for smaller y, or (d) cation vacancies as in $Tl_{2-y}Ba_2Ca_{n-1}Cu_nO_{2n+4-x}$ for larger $y \approx 0.5$. Proper characterization of the Tl_2 family by wet-chemical methods has demonstrated that the Tl_2 family differs from the Bi_2 family; the former has oxygen vacancies in the $Tl_{2-y}O_{2-x}$ layers while the latter has oxygen excess in the Bi_2O_{2+x} layers.

(5) Superconductivity occurs in a narrow mixed-valent composition between an antiferromagnetic semiconductor ($W < U$) and a normal metal ($W > U$) composition within a structurally single phase field. In the superconductive region the unusual conditions $W \approx U$, $W \approx 8\hbar\omega_R$, and $E_M \approx E_I$—where E_M and E_I are respectively the electrostatic Madelung stabilization energy and the energy required to create ions of the point charge model—all appear to be satisfied. An abrupt increase in the basal plane $(a + b)/2$ or c-axis Cu–O distance occurs on passing from the superconductive to the antiferromagnetic, semiconductive region due to an important localization of the Cu–3*d* electrons. These observations indicate the presence of an electronic instabil-

ity of the normal state of the mixed valent superconductors that is a prerequisite of high-T_c superconductivity.

Acknowledgments

We gratefully acknowledge the support for this research by the National Science Foundation and the Texas Advanced Research Program. We thank C. C. Torardi for Figs. 15 and 16.

References

1. J. B. GOODENOUGH, *Supercond. Sci. Technol.* **3,** 26 (1990).
2. J. B. GOODENOUGH AND J. ZHOU, *Phys. Rev. B,* in press.
3. A. MANTHIRAM AND J. B. GOODENOUGH, "Advances in the Synthesis and Reactivity of Solids" (T. E. Mallouk, Ed.), Vol. 1, in press, Jai Press, Greenwich, CT (1990).
4. J. M. LONGO AND P. M. RACCAH, *J. Solid State Chem.* **6,** 526 (1973); B. GRANDE, H. MÜLLER-BUSCHBAUM, AND M. SCHWEIZER, *Z. Anorg. Allg. Chem.* **428,** 120 (1977).
5. G. DEMAZEAU, F. TRESSE, TH. PLANTE, B. CHEVALIER, J. ETOURNEAU, C. MICHEL, M. HERVIEU, B. RAVEAU, P. LEJAY, A. SULPICE, AND T. TOURNIER, *Physica C* **153–155,** 824 (1988).
6. E. SCHIRBER, B. MOROSIN, R. M. MERILL, P. F. HLAVA, E. L. VENTURINI, J. F. KURAK, P. J. NIGREY, R. J. BAUGHMAN, AND D. S. GINLEY, *Physica C* **152,** 121 (1988).
7. J. ZHOU, S. SINHA, AND J. B. GOODENOUGH, *Phys. Rev. B* **39,** 12331 (1988).
8. C. CHAILLOUT, S. W. CHEONG, Z. FISK, M. S. LEHMAN, M. MAREZIO, B. MOROSIN, AND J. E. SCHIRBER, *Physica C* **158,** 183 (1989).
9. J. D. JORGENSEN, B. DABROWSKI, SHIYOU PEI, D. G. HINKS, AND L. SODERHOLM, *Phys. Rev. B* **38,** 11,337 (1988).
10. H. MÜLLER-BUSCHBAUM AND W. Z. WALLSCHLAGER, *Z. Anorg. Allg. Chem.* **414,** 76 (1975).
11. G. H. KEWEI, S.-W. CHEONG, Z. FISK, F. H. GARZON, J. A. GOLDSTONE, AND J. D. THOMPSON, *Phys. Rev. B* **40,** 9370 (1989).
12. E. TAKAYAMA-MUROMACHI, Y. MATSUI, Y. UCHIDA, F. IZUMI, M. ONODA, AND K. KATO, *Japan. J. Appl. Phys.* **27,** L2283 (1988).
13. H. SAWA, S. SUZUKI, M. WATANABE, J. AKIMITSU, H. MATSUBARA, H. WATABE, S. UCHIDA, K. KOKUSHO, H. ASANO, F. IZUMI, AND E. TAKAYAMA-MUROMACHI, *Nature (London)* **337,** 347 (1989).
14. S.-W. CHEONG, Z. FISK, J. D. THOMPSON, AND R. B. SCHWARZ, *Physica C* **159,** 407 (1989).
15. A. MANTHIRAM AND J. B. GOODENOUGH, *J. Solid State Chem.,* in press.
16. R. D. SHANNON, *Acta Crystallogr., Sect. A* **32,** 751 (1976).
17. J. F. BRINGLEY, S. S. TRAIL, AND B. A. SCOTT, *J. Solid State Chem.,* **86,** 310 (1990).
18. S. W. CHEONG, J. D. THOMPSON AND Z. FISK, Physica C **158,** 109 (1989).
19. I. S. SHAPLYGIN, B. R. KAKHAN, AND V. B. LAZAREV, *Russ. J. Inorg. Chem.* **24,** 820 (1979).
20. N. NGUYEN, J. CHOISNET, M. HERVIEU, AND B. RAVEAU, *J. Solid State Chem.* **39,** 120 (1981).
21. R. M. FLEMING, B. BATLOGG, R. J. CAVA, AND E. A. RIETMAN, *Phys. Rev. B* **35,** 7191 (1987).
22. M. W. SHAFER, T. PENNEY, AND B. L. OLSON, *Phys. Rev. B* **36,** 4067 (1987); J. B. TORRANCE, Y. TOKURA, A. I. NAZZAL, A. BEZINGE, T. C. HUANG, AND S. S. P. PARKIN, *Phys. Rev. Lett.* **61,** 1127 (1988).
23. S. UCHIDA, *in* "Proceedings of the IXth Winter Meeting on Low-Temperature Physics—Progress in High-Temperature Superconductivity" (J. Heiras, R. A. Barris, T. Akathi, and J. Tagüeña, Eds.), Vol. 5, p. 63, World Scientific, Singapore (1988).
24. Z. Z. WANG, J. CLAYHOLD, N. P. ONG, J. M. TARASCON, L. H. GREENE, W. R. MCKINNON, AND G. W. HULL, *Phys. Rev. B* **36,** 7222 (1987).
25. H. TAKAGI, S. UCHIDA, AND Y. TOKURA, *Physica C* **162–164,** 1677 (1989).
26. J. B. GOODENOUGH, A. MANTHIRAM, AND J. ZHOU, *Mater. Res. Soc. Symp. Proc.* (J. B. Torrance *et al.,* Eds.), Vol. 156, p. 239, Materials Research Society, Pittsburgh, PA (1989).
27. J. B. TORRANCE, A. BEZINGE, A. I. NAZZAL, T. C. HUANG, S. S. P. PARKIN, D. J. KEANE, S. J. LAPLACA, P. M. HORN, AND G. A. HEALD, *Phys. Rev. B* **40,** 8872 (1989).
28. R. BIRGENEAU, D. R. GABBE, H. P. JENSSEN, M. A. KASTNER, P. J. PICONE, T. R. THURSTON, G. SHIRANE, Y. ENDOH, M. SATO, K. YAMADA, Y. HIDAKA, M. ODA, Y. ENOMOTO, M. SUZUKI, AND T. MURAKAMI, *Phys. Rev. B* **38,** 6614 (1988).
29. A. WEIDINGER, CH. NIEDERMAYER, A. GOLNIK, R. SIMON, E. RECKNAGEL, J. I. BUDNICK, B. CHAMBERLAND, AND C. BAINES, *Phys. Rev. Lett.* **62,** 102 (1988).
30. T. TSUDA, T. SHIMIZU, H. YASUOKA, K. KISHIO, AND K. KITAZAWA, *J. Phys. Soc. Japan* **57,** 2908 (1987).
31. K. KUMAGI AND Y. NAKAMURA, *Physica C* **157,** 307 (1989).

32. F. J. HIMPSEL, G. V. CHANDRASHEKHAR, A. B. MCLEAN, AND M. W. SHAFER, *Phys. Rev. B* **38,** 11,946 (1988).
33. J. B. GOODENOUGH, *J. Mater. Educ.* **9,** 620 (1987).
34. J. R. COOPER, B. ALAVI, L.-W. ZHOU, W. P. BEYERMANN, AND G. GRÜNER, *Phys. Rev. B* **35,** 8794 (1987).
35. C. UHER, A. B. KAISER, E. GMELIN, AND L. WALZ, *Phys. Rev. B* **36,** 5676 (1987).
36. Y. ANDO, M. SERA, S. YAMAGATA, S. KONDOH, N. ONODA, AND M. SATO, *Solid State Commun.* **70,** 303 (1989).
37. F. DEVAUX, A. MANTHIRAM, AND J. B. GOODENOUGH, *Phys. Rev. B,* **41,** 8723 (1990).
38. A. K. BHATNAGAR, R. PAN, D. G. NAUGLE, G. R. GILBERT, AND R. K. PANDEY, *Phys. Rev. B* **41,** 4002 (1990).
39. M. F. HUNDLEY, J. D. THOMPSON, S. W. CHEONG, Z. FISK, AND J. E. SCHIRBER, *Phys. Rev. B* **41,** 4062 (1990).
40. P. M. GRANT, S. S. P. PARKIN, V. Y. LEE, E. M. ENGLER, M. L. RAMIREZ, J. E. VAZQUEZ, G. LIM, R. D. JACOWITZ, AND R. L. GREENE, *Phys. Rev. Lett.* **58,** 2482 (1987).
41. J. W. ROGERS, JR., N. D. SHINN, J. E. SCHIRBER, E. L. VENTURINI, D. S. GINLEY, AND B. MOROSIN, *Phys. Rev. B* **38,** 5021 (1988).
42. J. D. JORGENSEN, B. DABROWSKI, SHIYOU PEI, D. R. RICHARDS, AND D. G. HINKS, *Phys. Rev. B* **40,** 2187 (1989).
43. J.B. GOODENOUGH AND A. MANTHIRAM, *Physica C* **157,** 439 (1989).
44. J. W. ALLEN, C. G. OLSON, M. B. MAPLE, J.-S. KANG, L. Z. LIU, J.-H. PARK, R. O. ANDERSON, W. P. ELLIS, J. T. MARKERT, Y. DALICHAUCH, AND R. LIU, *Phys. Rev. Lett.* **64,** 595 (1990).
45. M. SUZUKI, *Phys. Rev. B* **39,** 2312 (1989).
46. G. M. LUKE *et al., Physica C* **162–164,** 825 (1989).
47. A. MANTHIRAM, X. X. TANG, AND J. B. GOODENOUGH, *Phys. Rev. B,* in press.
48. N. F. MOTT AND E. A. DAVIS, "Electronic Processes in Non-crystalline Materials," 2nd ed., Oxford Univ. Press, Oxford (1979).
49. J. D. JORGENSEN, B. W. VEAL, A. P. PAULIKAS, L. J. NOWICKI, G. W. CRABTREE, H. CLAUS, AND W. K. KWOK, *Phys. Rev. B* **41,** 1863 (1990).
50. H. SAWA, K. OBARA, J. AKIMITSU, Y. MATSUI, AND S. HORIUCHI, *J. Phys. Soc. Japan* **58,** 2252 (1989).
51. F. IZUMI, H. KITO, H. SAWA, J. AKIMITSU, AND H. ASANO, *Physica C* **160,** 235 (1989).
52. W. WONG-NG, F. W. GAYLE, D. L. KAISER, S. F. WATKINS, AND F. R. FRONCZEK, *Phys. Rev. B* **41,** 4220 (1990).
53. A. MANTHIRAM, J. S. SWINNEA, Z. T. SUI, H. STEINFINK, AND J. B. GOODENOUGH, *J. Amer. Chem. Soc.* **109,** 6667 (1987).
54. R. J. CAVA, B. BATLOGG, C. H. CHEN, E. A. RIETMAN, S. M. ZAHURAK, AND D. WEIDER, *Nature (London)* **329,** 423 (1987); *Phys. Rev. B* **36,** 5619 (1987).
55. B. T. AHN, T. M. GÜR, R. A. HUGGINS, R. BEYERS, E. M. ENGLER, P. M. GRANT, S. S. P. PARKIN, G. LIM, M. L. RAMIREZ, K. P. ROCHE, J. E. VAZQUEZ, V. Y. LEE, AND R. D. JACOWITZ, *Physica C* **153–155,** 590 (1988).
56. C. J. HOU, A. MANTHIRAM, L. RABENBERG, AND J. B. GOODENOUGH, *J. Mater. Res.* **5,** 9 (1990).
57. J. B. GOODENOUGH, "Proceedings of High-T_c Superconductors: Magnetic Interactions—Progress in High Temperature Superconductivity" (L. H. Bennett, Y. Flom, and G. C. Vezzoli, Eds.), Vol. 17, p. 41, World Scientific, Singapore (1989).
58. Y. J. UEMURA *et al., Phys. Rev. Lett.* **62,** 2317 (1989).
59. C. CHAILLOUT, M. B. ALARIO-FRANCO, J. J. CAPPONI, J. CHENAVAS, P. STROBEL, AND M. MAREZIO, *Solid State Commun.* **65,** 283 (1988).
60. W. K. HAM, S. W. KELLER, J. N. MICHAELS, A. M. STACY, D. KRILLOV, D. T. HODUL, AND R. H. FLEMING, *J. Mater. Res.* **4,** 504 (1989).
61. M. CARDONA, R. LIU, C. THOMSEN, W. KRESS, S. SCHONHERR, M. BAUER, L. GENZEL, AND W. KÖNIG, *Solid State Commun.* **67,** 789 (1988).
62. C. NAMGUNG, J. T. S. IRVINE, J. S. BINKS, AND A. R. WEST, *Supercond. Sci. Technol.* **1,** 169 (1988); J. D. JORGENSEN, H. SHAKED, D. G. HINKS, B. DABROWSKI, B. W. VEAL, A. P. PAULIKAS, L. J. NOWICKI, G. W. CRABTREE, W. K. KWOK, L. H. NIMEZ, AND H. CLAUS, *Physica C* **153–155,** 578 (1988).
63. A. MANTHIRAM AND J. B. GOODENOUGH, *Nature (London)* **329,** 701 (1987).
64. Y. DAI, A. MANTHIRAM, A. CAMPION, AND J. B. GOODENOUGH, *Phys. Rev. B* **38,** 5091 (1988).
65. A. MANTHIRAM, S. J. LEE, AND J. B. GOODENOUGH, *J. Solid State Chem.* **73,** 278 (1988).
66. A. MANTHIRAM, X. X. TANG, AND J. B. GOODENOUGH, *Phys. Rev. B* **37,** 3734 (1988).
67. A. MANTHIRAM AND J. B. GOODENOUGH, *Physica C* **162–164,** 69 (1989).
68. A. MANTHIRAM AND J. B. GOODENOUGH, *Physica C* **159,** 760 (1989).
69. K. TAKITA, H. AKINAGA, H. KATOH, H. ASANO, AND K. MASUDA, *Japan. J. Appl. Phys.* **27,** L67 (1988).
70. K. TAKITA, H. AKINAGA, H. KATOH, AND K. MASUDA, *Japan. J. Appl. Phys.***27,** L1676 (1988).

71. J. M. TARASCON, W. R. MCKINON, L. H. GREENE, G. W. HULL, AND E. M. VOGEL, *Phys. Rev. B* **36,** 226 (1987).
72. A. MATSUDA, K. KINOSHITA, T. ISHII, H. SHIBATA, T. WATANABE, AND T. YAMADA, *Phys. Rev. B* **38,** 2910 (1988).
73. J.-S. KANG, J. W. ALLEN, Z. X. SHEN, W. P. ELLIS, J. J. YEH, B. W. LEE, M. B. MAPLE, W. E. SPICER, AND I. LINDAU, "Proc. 18th Rare Earth Research Conference, Lake Geneva, Wisconsin, Sept. 12–16, 1988."
74. E. E. ALP, L. SODERHOLM, G. K. SHENOY, D. G. HINKS, B. W. VEAL, AND P. A. MONTANO, *Physica B* **150,** 74 (1988).
75. S. HORN, J. LAI, S. A. SHAKEN, Y. JEON, M. CROFT, C. L. CHANG, AND M. L. DEN BOER, *Phys. Rev. B* **36,** 3895 (1988); U. NEUKRICH, C. T. SIMMONS, P. SLADECZEK, C. LAUBSCHAT, O. STROBEL, G. KAINDL, AND D. D. SARMA, *Europhys. Lett.* **5,** 567 (1988).
76. A. P. GONCALVES, I. C. SANTOS, E. B. LOPES, R. T. HENRIQUES, M. ALMEIDA, AND M. O. FIGUEIREDO, *Phys. Rev. B* **37,** 747 (1988).
77. J. J. NEUMEIER, M. B. MAPLE, AND M. S. TARIKACHVILLI, *Physica C* **156,** 574 (1988).
78. X. X. TANG, A. MANTHIRAM, AND J. B. GOODENOUGH, *Physica C* **161,** 574 (1989).
79. Y. TOKURA, A. FUJIMORI, H. MATSUBARA, H. WATABE, H. TAKAGI, S. UCHIDA, M. SAKAI, H. IKEDA, S. OKUDA, AND S. TANAKA, *Phys. Rev. B* **39,** 9704 (1989).
80. J. J. NEUMEIER, T. BJØRNHOLM, M. B. MAPLE, AND I. K. SHULLER, *Phys. Rev. Lett.* **63,** 2516 (1989).
81. X. X. TANG, A. MANTHIRAM, AND J. B. GOODENOUGH, unpublished.
82. M. A. SUBRAMANIAN, J. C. CALABRESE, C. C. TORARDI, J. GOPALAKRISHAN, T. R. ASKEW, R. B. FLIPPEN, K. J. MORRISSEY, U. CHOWDHRY, AND A. W. SLEIGHT, *Nature (London)* **332,** 420 (1988).
83. C. C. TORARDI, M. A. SUBRAMANIAN, J. C. CALABRESE, J. GOPALAKRISHNAN, E. M. MCCARRON, K. J. MORRISSEY, T. R. ASKEW, R. B. FLIPPEN, U. CHOWDHRY, AND A. W. SLEIGHT, *Phys. Rev. B* **38,** 225 (1988).
84. M. A. SUBRAMANIAN, C. C. TORARDI, J. C. CALABRESE, J. GOPALAKRISHNAN, K. J. MORRISSEY, T. R. ASKEW, R. B. FLIPPEN, U. CHOWDHRY, AND A. W. SLEIGHT, *Science* **239,** 1015 (1988).
85. C. C. TORARDI, M. A. SUBRAMANIAN, J. C. CALABRESE, J. GOPALAKRISHNAN, K. J. MORRISSEY, T. R. ASKEW, R. B. FLIPPEN, U. CHOWDHRY, AND A. W. SLEIGHT, *Science* **240,** 631 (1988).
86. M. KIKUCHI, S. NAKAJIMA, Y. SYONO, K. HIRAGA, T. OKU, D. SHINDO, N. KOBAYASHI, H. IWASAKI, AND Y. MUTO, *Physica C* **158,** 79 (1989).
87. S. S. P. PARKIN, V. Y. LEE, A. I. SAVOY, R. BEYERS, AND S. J. LAPLACA, *Phys. Rev. Lett.* **61,** 750 (1988).
88. H. IHARA, R. SUGISE, K. HIRABAYASHI, N. TERADA, M. JO, K. HAYASHI, A. NEGISHI, M. TOKUMOTO, Y. KIMURA, AND T. SHIMOMURA, *Nature (London)* **334,** 510 (1988).
89. H. IHARA, R. SUGISE, K. HAYASHI, N. TERADA, M. JO, M. HIRABAYASHI, N. NEGISHI, N. ATODA, H. OYANAGI, T. SHIMOMURA, AND S. OSHASHI, *Phys. Rev. B* **38,** 11,952 (1988).
90. P. HALDAR, K. CHEN, B. MAHESWARAN, A. ROIG-JANICKI, N. K. JAGGI, R. S. MARKIEWICZ, AND B. C. GIESSEN, *Science* **241,** 1198 (1988).
91. B. W. STATT, Z. WANG. M. J. G. LEE, J. V. YAKHMI, P. C. DECAMARGO, AND J. G. RUTTER, *Physica C* **156,** 251 (1988).
92. M. D. KIRK, J. NOGAMI, A. A. BASKI, D. B. MITZI, A. KAPITULNIK, T. H. GEBALLE, AND C. F. QUATE, *Science* **242,** 1673 (1988).
93. C. C. TORARDI, D. JUNG, D. B. KANG, J. REN, AND M.-H. WHANGBO, "Mater. Res. Soc. Symp. Proc.," (J. B. Torrance *et al.*, Eds.), Vol. 156, Materials Research Society, Pittsburgh, PA (1989).
94. J. REN, D. JUNG, M.-H. WHANGBO, J. M. TARASCON, Y. LEPAGE, W. R. MCKINNON, AND C. C. TORARDI, *Physica C* **159,** 151 (1989).
95. A. MANTHIRAM AND J. B. GOODENOUGH, *Appl. Phys. Lett.* **53,** 420 (1988).
96. C. C. TORARDI, J. B. PARISE, M. A. SUBRAMANIAN, J. GOPALAKRISHNAN, AND A. W. SLEIGHT, *Physica C* **157,** 115 (1989).
97. S. J. HIBBLE, A. K. CHEETHAM, A. M. CHIPPINDALE, P. DAY, AND J. A. HRILJAC, *Physica C* **156,** 604 (1988).
98. M. PARANTHAMAN, A. MANTHIRAM, AND J. B. GOODENOUGH, *J. Solid State Chem.*, in press.
99. Y. SHIMAKAWA, Y. KUBO, T. MANAKO, T. SATOH, S. IIJIMA, T. ICHIHASHI, AND H. IGARASHI, *Physica C* **157,** 279 (1989).
100. S. J. HIBBLE, B. K. CHEETHAM, A. M. CHIPPENDALE, P. DAY, AND J. A. HRILJAE, *Physica C,* **156,** 604 (1988).
101. S. NAKAJIMA, M. KIKUCHI, T. OKU, N. KOBAYASHI, T. SUZUKI, K. NAGASE, K. HIRAGA, Y. MUTO, AND Y. SYONO, *Physica C* **160,** 458 (1989).
102. T. SUZUKI, M. NAGOSHI, Y. FUKUDA, Y. SYONO, M. KIKUCHI, N. KOBAYASHI, AND M. TACHIKI, *Phys. Rev. B* **40,** 5184 (1989).
103. D. R. HAMANN AND L. F. MATTHEISS, *Phys. Rev. B* **38,** 5138 (1988).

104. D. JUNG, M.-H. WHANGBO, N. HERRON, AND C. C. TORARDI, *Physica C* **160,** 381 (1989).

105. J. B. PARISE, C. C. TORARDI, M. A. SUBRAMANIAN, J. GOPALAKRISHNAN, A. W. SLEIGHT, AND E. PRINCE, *Physica C* **159,** 239 (1989).

106. J. B. PARISE, N. HERRON, M. K. CRAWFORD, AND P. L. GAI, *Physica C* **159,** 255 (1989).

107. I. M. KOLTHOFF AND R. BELCHER, "Volumetric Analysis III," p. 370, Interscience, New York (1957).

108. E. H. APPELMAN, L. R. MORSS, A. M. KINI, U. GEISER, A. UMEZAWA, G. W. CRABTREE, AND K. D. CARLSON, *Inorg. Chem* **26,** 3237 (1987).

109. A. MANTHIRAM, M. PARANTHAMAN, AND J. B. GOODENOUGH, *Physica C,* submitted for publication.